UNIVERSITY OF OKLAHOMA

GRADUATE COLLEGE

# MODELING MICROEMULSION PHASE BEHAVIOR WITH CONSIDERATION OF PHASE PARTITIONING OF CO-SOLVENT

A THESIS

SUBMITTED TO THE GRADUATE FACULTY

in partial fulfillment of the requirements for the

Degree of

MASTER OF SCIENCE IN NATURAL GAS ENGINEERING AND MANAGEMENT

By

BINBIN MU
Norman, Oklahoma
2017

MODELING MICROEMULSION PHASE BEHAVIOR WITH CONSIDERATION OF PHASE PARTITIONING OF CO-SOLVENT

A THESIS APPROVED FOR THE
MEWBOURNE SCHOOL OF PETROLEUM AND GEOLOGICAL ENGINEERING

BY

_____
Dr. Ahmad Jamili, Chair

_____
Dr. Bor-Jier (Ben) Shiau

_____
Dr. Xingru Wu

*I dedicate my thesis work to my family and many friends. A special feeling of gratitude to my loving mother, Xiaojun Lin, who has always loved me unconditionally and whose words of encouragement and push for tenacity ring in my ears.*

*I also dedicate this thesis to many of my friends who have supported me throughout the process. I will always appreciate all they have done, especially Dongqi Wen for helping me develop my technology skills, and for the many hours of proofreading.*

## Acknowledgements

It is such a great luck and honor for me that I have performed my graduate work at a university as collaborative as the University of Oklahoma; therefore, there are many people to thank for their part in my thesis work. I would first like to express my gratitude to my thesis advisor Dr. Ahmad Jamili for his advice and support on my research. His generous guidance and understanding made it possible for me to work on a topic that was of great interest to me. It was a pleasure working with him. I would like to thank my course advisor Dr. Suresh Sharma. The door to Prof. Sharma's office was always open whenever I ran into a trouble spot or had a question. I would also like to show my gratitude to Dr. Bor-Jier (Ben) Shiau and Dr. Xingru Wu for comments that greatly improved the manuscript.

This thesis cannot be accomplished without the help of Dr. Luchao Jin. I want to express my appreciation to him for his advice and teachings on phase behavior modeling, UTCHEM, and advancing our cooperated projects. It was a pleasure to work on the HLD-NAC model and writing publications together with him.

Finally, I profoundly appreciate everyone helping me throughout my graduate study. I would have never been able to complete my graduate study without their help.

# Table of Contents

# List of Tables

# List of Figures

# Abstract

Co-solvents are widely used to improve chemical flooding formulations design, but partitioning of co-solvent within phases has great impacts on microemulsion phase behavior. Microemulsion phase behavior plays a key role in surfactant flooding processes. Therefore, it is critical to accurately model microemulsion phase behavior with the consideration of co-solvent phase partitioning in a compositional chemical flooding simulation.

The physics based Hydrophilic Lipophilic Difference and Net Average Curvature (HLD-NAC) equation of state (EOS) coupled with the thermodynamic-based co-solvent partitioning model was developed in this work to model microemulsion phase behavior for the systems contained co-solvents.

Five microemulsion systems were used to examine the developed approach. Solubilization ratios under salinity scan of these systems were reproduced. The matching length parameters were underestimated for each system by assuming all co-solvents were completely adsorbed at the phase interface instead of using the co-solvent partitioning model. However, length parameters were more physically representing the actual surfactant tail lengths when determined by the developed model. The results proved that the improved HLD-NAC model which accounted the co-solvent partitioning model can accurately simulate phase behavior of surfactant/ co-solvent/oil/ brine systems.

The improved HLD-NAC model then was used to determine the length parameter for the system consisted of brine, n-decane, 1.5% of Witco TRS 10-410 and 1.5% of isobutyl alcohol (IBA). After determination of length parameter,

catastrophic phase inversion theory and Khorsandi and Johns's flash algorithm coupled with co-solvent partitioning model were employed to reproduce the binodal curves based on experimental data. And then, the accuracy of the model binodal curves was examined. The model binodal curves created by catastrophic phase inversion theory were not able to reproduce the experimental binodal curves for the system to acceptable extent. Significant errors may occur when estimating the number of phases and the concentrations of compositions in microemulsion phase with the plotted ternary diagrams. However, the Khorsandi and Johns' flash algorithm with consideration of co-solvent phase partitioning can accurately simulate phase behavior for all Winsor type microemulsions. The results proved that the new algorithm can make better model binodal curves in the ternary diagrams of the surfactant/co-solvent/crude oil/brine systems. A flow chart for the new algorithm as well as the results of tuning parameters were presented and demonstrated in this work.

# Chapter 1: Introduction

There are normally three categories of methods to recover crude oil reservoirs. The first category is the primary recovery methods, which mainly using gas pressure, expanding force of rock layers, and other natural forces in the reservoirs to recover crude oil. Secondary recovery methods fall in the second category. Water flooding is one of the well-established technologies in this category. Generally, the overall oil recovery of a reservoir with the combination of primary and secondary methods is approximately one-third of the total crude oil in this reservoir. A large amount of residual oil can be potentially squeezed out of the ground if appropriate methods applied. These methods are known as tertiary oil recovery methods. Surfactant flooding is one of the tertiary oil recovery methods, in which surfactants are added to aqueous solution to reduce the amount of residual oil.

Coreflood experiments have proven that residual oil saturation after displacement of water can range from 15% to 40%. However, surfactant flooding after the waterflood can further reduce the residual oil saturation to less than 5% (Lu et al. 2014a). The reason for the high residual oil saturation in water flooding is the capillary trapping of oil at the pore throats in the porous media due to water is the wetting phase in most sandstone reservoirs. It has been realized that the residual oil saturation is relative to a dimensionless parameter, capillary number $N_c = \mu v/(IFT)$; where $\mu$ is the viscosity of aqueous solution, $v$ is the interstitial velocity, and $IFT$ is the oil-water interfacial tension (Taber 1969; Stegemeier 1977; Melrose 1974; Foster 1973). The relationship between capillary number

and residual oil saturation is that residual oil saturation can be reduced to below 5%, when the capillary number increases from $10^{-5}$ to $10^{-2}$ magnitude (Abrams 1975). Surfactants have the capability to increase the capillary number by decreasing the oil-water IFT, thus to reduce the residual oil saturation.

Surfactant flooding processes have been well established for decades. In order to apply surfactant flooding to various reservoirs of interest, researchers have studied and refined different new surfactants and formulations. The first step of a general surfactant flooding process is to screen a candidate reservoir which is suitable for surfactant flooding. Once the reservoir conditions are determined, researchers are able to design the formulations according to the reservoir brine salinity, temperature and oil properties. And then conduct coreflood experiments with designed formulations to evaluate the displacement efficiency, followed by coreflood simulation so as to obtain the coreflood's results and parameters which can represent the multiphase displacement process. Finally, pilot test simulation can be conducted with the inputs which are the parameters obtained from the coreflood simulation to predict the oil recovery in field scale, thus the economics can be evaluated.

Microemulsion phase behavior plays a key role in surfactant flooding processes. In formulation design, researcher conduct microemulsion phase behavior tests to screen candidate surfactant and optimize the surfactant formulation. Different microemulsion types lead to different displacement mechanisms, thus different displacement efficiencies in coreflood process. Type III microemulsion can reduce the oil-water IFT and mobilize the residual oil most

efficiently. And in coreflood simulation, phase composition, phase saturation and IFT are all functions of microemulsion phase behavior. Therefore, a correct phase behavior model is critical to the results of surfactants flooding simulations.

Even though many surfactants can achieve an ultra-low IFT, sometimes they are not sufficiently soluble at optimum salinity to reach the aqueous stability. Thus, co-solvents such as alcohols are often used as additional components in the formulations to make the primary surfactants sufficiently soluble in the brine. Co-solvents are playing an important role in letting the formulations reach the desired aqueous stability. Furthermore, the additional advantages of using co-solvents in the formulations are their capacities to reduce the bending modulus which lessens the microemulsion viscosity and Newtonian behavior, and to break macroemulsions into microemulsion resulting in a reduction of the required time to coalesce or equilibrate the microemulsion. Co-solvents are widely used to improve chemical flooding formulation design, but their partitioning within phases has great impacts on microemulsion phase behavior. Therefore, in order to correctly predict oil recovery and better evaluate the performance of designed formulations, it is critical to accurately model microemulsion phase behavior with phase partitioning of co-solvent in a compositional chemical flooding simulation.

All co-solvents were used to assume to be completely dissolved and adsorbed at the phase interface. However, this assumption led to an overestimated interfacial area, thus an underestimated length parameter for the formulation with co-solvents. This work aims to exercise Hydrophilic-Lipophilic Deviation and Net-Average Curvature (HLD-NAC) equation of state (EOS) with the

consideration of co-solvent partitioning within all phases to address this problem. This study further correlates the co-solvent partitioning model with the Khorsandi and John's flash algorithm to substitute the catastrophic phase inversion theory to create the continuous binodal curves for the systems contained co-solvents.

In this thesis, Chapter 2 presents a survey of the studies about modeling microemulsion phase behaviors and co-solvents partitioning. Important concepts and detail equations for HLD-NAC EOS and the Biais' (1981) and Hirasaki's (1982) model for co-solvent partitioning are also introduced in order to prepare for further discussion of combination of these two models.

Chapter 3 combines the HLD-NAC model with the co-solvent partitioning model to reproduce the solubilization ratio curves from experiment results for five microemulsion systems by adjusting the surfactant tail length parameters for each system. Details of the five systems, including chemical formulations, oil properties and properties of surfactants and co-solvents, are presented. Further, this chapter also describes two methods, catastrophic phase inversion theory and Khorsandi and Johns's flash algorithm (2016), to create model binodal curves.

In Chapter 4, solubilization ratio curves for five microemulsion systems are presented to validate that the method developed in Chapter 3. This method is able to compute more accurate surfactant tail length parameters for each system. Since co-solvents have great effects on the length parameters, discussion for the results of the length parameters focuses on the comparison between the assumption that all co-solvents completely partition into the microemulsion phase and the fact that co-solvents partition within all phases.

After the inspection of length parameters, the chapter employs the catastrophic phase inversion theory and Khorsandi and Johns's flash algorithm coupled with co-solvent partitioning model to reproduce the binodal curves based on experimental data for the system consisted of brine, n-decane, 1.5% of Witco TRS 10-410 and 1.5% of IBA. The length parameter for this system is calculated by using the method developed in Chapter 3, so that the error generated by length parameter can be eliminated. Finally, accuracy of the model binodal curves is examined.

Chapter 5 summarizes the conclusions of this work.

# Chapter 2: Literature Review

One of the well-established technologies in Enhanced Oil Recovery (EOR) is surfactant flooding. Its mechanism is mainly that a surfactant lowers the oil-brine interfacial tension (IFT) so that the amount of residual oil saturation can be reduced. Phase behavior tests are generally used in the formulation design process to obtain a balanced and stable system with ultralow oil-brine IFT ($10^{-3}$ mN/m). When the IFTs are at ultralow values, the reservoir displacements are at optimum conditions (Nelson and Pope 1978).

Physical properties of chemical flooding such as microemulsion viscosities, surfactant adsorptions, phase relative permeabilities as well as IFTs are functions of phase compositions and saturations (Prouvost et al. 1984, Delshad et al. 1996). Phase compositions need to be determined by modeling microemulsion phase behavior for the systems. Parameters, such as oil equivalent alkane carbon number (EACN), salinity, co-surfactants, surfactant hydrophobicity, and temperature, have significant effects on the microemulsion phase behavior (Green and Willhite 1998). A high accurate model for microemulsion phase behavior in a surfactant/oil/brine system is important to surfactant flooding simulation. A proper phase behavior model should be developed and tuned by matching lab data of phase behavior, such as solubilizaiton ratio curves and IFTs. Once the model is set, it can be used to predict the microemulsion phase behavior in the reservoir condition.

There have been different models, either empirical or physical, describing microemulsion phase behaviors. One of the most famous empirical models is

Hand's rule (Hand 1939). Although Hand's rule has been widely used for decades, it does have some significant drawbacks. For example, Hand's rule does not take physical properties of surfactants into account. Further, Hand's rule requires at least five empirical parameters to match experimental data before successfully modeling microemulsion phase behavior as a function of salinity. Additional matching parameters may be required if other effects are introduced to the model (Delshad et al. 1996). One, who wants to solve the Hand's rule equations, needs to make initial guesses for phase compositions and to perform calculation iteratively (Sheng 2010). However, the solving processes could be burdensome and the results could have significant errors, since there are so many uncertain parameters needed to be matched with the lab data of phase behavior. Therefore, these empirical features of Hand's rule lower the capability of the model in predicting microemulsion phase behavior.

Generally, there are three types of microemulsion categorized by the structure of micelles and the composition of excess phases: Winsor Type I, Winsor Type II, and Winsor Type III (Winsor 1948). The affinity of the surfactant to oil and brine water phases qualitatively describes the Winsor types. Research of Mitchell and Nihanm (1981) in the geometry of interfacial surfactant layer presented one of the most typical physical model studies in microemulsion phase behavior. This model was further improved by Chou and Bae (1988). They accounted for the effects of salinity, surfactant structure, alcohol and EACN so that the phase behavior model became appropriate for high salinity surfactant formulations. By adjusting three parameters, which are related to the

characteristic of each component, the model was able to predict the microemulsion transition with increasing salinity. Additionally, these three parameters from one specific system, once determined, can be applied to another system. Although this physical phase behavior model seems to outperform the Hand's rule in high salinity environment, it is only valid in high salinity condition, and it has never been applied for phase behavior tests with crude oils. Consequently, the models have been mentioned so far, providing limited accuracy for microemulsion phase behavior in chemical flooding.

Another physically based phase behavior model, HLD-NAC, has been developed by Acosta et al. (2003). This model consists of two parts: one part is the Hydrophilic Lipophilic Difference (HLD) equation for designing optimum formulation; the other part is the Net-Average Curvature (NAC) concept for predicting microemulsion phase behavior.

## 2.1 HLD-NAC

### *2.1.1 HLD Equation for Predicting Optimum Formulation*

The first part of HLD-NAC model is the Hydrophilic Lipophilic Difference (HLD) equation proposed by Salager et al. (1979, 1999). HLD considers the effects of salinity, EACN, surfactant characteristic curvature ($Cc$) and correlates them into the model. HLD can be expressed as below,

$$HLD = \ln(S) - K \times EACN - \alpha_T \Delta T + Cc + f(A) \quad (1)$$

Where, $S$ is the salinity $(g/100\,ml)$. $EACN$ is the equivalent alkane carbon number of the oil. $K$ is the slope of the logarithm of optimum salinity as a function of $EACN$. $f(A)$ is a function of alcohol type and concentration. $Cc$ is the

characteristic parameter of surfactant. $\alpha_T$ is the temperature coefficient of optimum salinity expressed in unit of $ln(S)$ per $K$; and $\Delta T$ is temperature difference from reference temperature in $K$.

Ghosh and Johns (2014) later added a pressure term $\beta \Delta P$ to predict the microemulsion phase behavior for live oil.

The physical meaning of HLD values is that how much free energy has changed when one surfactant molecule transferred from the oil phase to the brine water phase (Salager et al. 2000a, Salager et al. 2000b), indicating the deviation from the optimum formulations. A positive HLD value represents the formation of Winsor Type II microemulsion, while a negative value corresponds to the formation of Winsor Type I microemulsion. If HLD equals to zero, Winsor Type III microemulsion is existing. The signs of each variable in Eq. 1 indicate how the specific variable affects the phase transition in the systems. If there is a positive sign in front of the variable, an increase in the value of that variable would lead to a Type I → Type III → Type II transition. However, a negative sign is associated with a Type II → Type III → Type I transition in the systems (Salager and Anton 1999). The values of $K$ range from 0.1 to 0.2, for numerous surfactants-oil combinations, but a value of 0.17 is typically used for most surfactants (Salager and Anton 1999). The factor $\alpha_T \Delta T$ is representing that the hydrogen bonds between water molecules become weaker as the temperature increases (Acosta et al. 2008). A usual value for $\alpha_T$ is $0.01\, K^{-1}$ for anionic surfactants (Salager and Anton 1999). Characteristic curvature ($Cc$) is the normalized net-curvature of the surfactant at reference condition (Acosta et al.

2008, Hammond and Acosta 2012). It represents the hydrophobicity of surfactant. If a $Cc$ value is negative, a surfactant, which forms normal micelles under the reference condition is in the system. However, if a $Cc$ value is greater than zero, a hydrophobic surfactant which produces reverse micelles is in the system. The HLD parameters, including $Cc$, $K$, and $\alpha_T$, are surfactant dependent, helping chemical flooding formulation design (Trahan et al. 2015). The formulation designers can rapidly narrow the choices of suitable surfactant systems that fit for field conditions with given oil EACN, reservoir temperature, salinity, and other HLD parameters. When HLD equals to zero, ultralow IFT is achieved; thus, the formulation is the optimum formulation for the system.

If some parameters in Eq. 1 are unknown, a salinity scan can help to determine the HLD value.

$$HLD = \ln(\frac{S}{S^*}) \quad (2)$$

Where, $S^*$ is the optimum salinity at which HLD equals to zero. Therefore, under optimum condition, Eq. 1 can be rearranged,

$$-\ln(S^*) = -K \times EACN - \alpha_T \Delta T + Cc + f(A) \quad (3)$$

### *2.1.2 NAC Concept for Predicting Microemulsion Phase Behavior*

Although HLD can express the quantity contributions of each factors, such as salinity, EACN, surfactant hydrophobicity, etc., to the transition of phase types, it contains no information about how much oil or brine water dissolved in the microemulsion phase. In order to identify the amount of oil or brine water in microemulsion phase, Acosta et al. (2003) introduced a Net-Average Curvature

(NAC) equation of state (EOS). The reason NAC EOS can calculate phase compositions is that NAC EOS assumes any microemulsion molecule could be considered as a hypothetical spherical droplet with oil and brine water coexisting, and the inverse of the radii of the oil and brine water droplets is the curvature of the microemulsion. The difference between the oil curvature and the brine water curvature is equivalent to the ratio of HLD and a length parameter $L$. This relationship is called net-curvature, and it can be mathematically described in Eq. 4. It has been proven that the length parameter $L$ is proportional to the extended length of the surfactant tail group (Acosta et al. 2003). Jin et al (2015) treated the length parameter as a matching parameter for large surfactant molecules.

$$H_n = \left|\frac{1}{R_o}\right| - \left|\frac{1}{R_w}\right| = \frac{-HLD}{L} \quad (4)$$

Where, $R_o$ and $R_w$ are the radii of coexisting hypothetical spherical aggregates of oil and brine water, respectively. $H_n$ is the curvature of the surfactant film adsorbed at the oil-brine interface. $L$ is the length parameter, which fully extended length of surfactant tail group. A positive $H_n$ value indicates a negative HLD value ($H_n > 0$ and $HLD < 0$), thus the radius of brine water is much greater than the radius of oil ($R_w \gg R_o$), and the system is Type I microemulsion. However, if $H_n$ is negative and HLD is positive ($H_n < 0$ and $HLD > 0$), the radius of oil is much greater than the radius of brine water ($R_o \gg R_w$), thus the system is Type II microemulsion. A zero net-curvature ($H_n = 0$ and $HLD = 0$) indicates the system is Type III microemulsion which contains approximately identical amounts of oil and brine water ($R_w \approx R_o$).

Since all brine water is assumed to dissolve in the microemulsion phase and the excess phase is only oil phase in Type I systems, and the contribution of surfactant molecules to the micellar volume is assumed to be ignorable, the hypothetical radius of brine water then can be computed by using the volume of bine in the system and the total surfactant area, which is shown as Eq. 5.

$$R_w = \frac{3 \times V_w}{A_s} \tag{5}$$

The oil hypothetical radius can be determined by Eq. 4 after the brine water hypothetical radius is calculated.

Similarly, in Type II microemulsion systems, all oil dissolved in the microemulsion phase, and the contribution of surfactant molecules to the micellar volume is ignored. Plus, the excess phase is only brine water. Thus, the hypothetical radius of oil is calculated by using the volume of oil in the system and the total surfactant area, which is shown as Eq. 6. And then, the brine water hypothetical radius then can be determined by Eq. 4.

$$R_o = \frac{3 \times V_o}{A_s} \tag{6}$$

$A_s$ is the interfacial area provided by the specific surfactant or co-solvent. It can be calculated as,

$$A_s = \sum V_w \frac{C_{s_i}}{MW_i} \times 6.023 \times 10^{23} \times a_{s_i} \times \rho_i \tag{7}$$

Where, $V_w$ is the volume of brine water in the system. $C_{s_i}$ is the concentration of each surfactant or co-solvent $i$. $MW_i$ is the molecular weight of the surfactant or co-solvent $i$. $a_{s_i}$ is the surface area per molecule of the surfactant or co-solvent $i$. And $\rho_i$ is the density of the surfactant or co-solvent $i$.

A typical characteristic of a surfactant, which consists of a hydrophilic head and a hydrophobic hydrocarbon tail, is the tendency to adsorb at interface. Eq. 7 is appropriate for two reason. The first reason is the fact that micelles, shown as Figure 1, start forming up once the surfactant concentration is greater than its Critical Micelle Concentration (CMC) in a surfactant/oil/brine system. Another reason is the assumption that there is no surfactant in monomer form (Acosta et al. 2003).

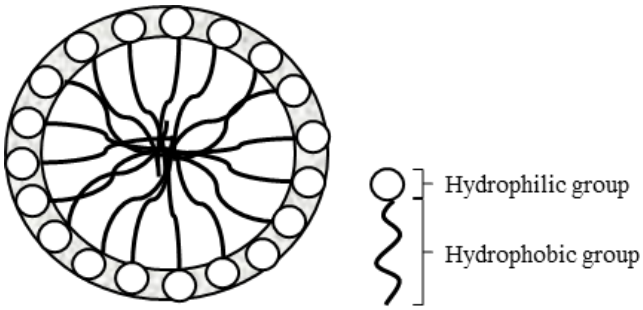


**Figure 1 Schematic of a spherical micelle**

Net-curvature equation can be used to calculate the oil and brine water hypothetical radii for either Type I or Type II system. However, it is not valid when the system is in Type III microemulsion because the oil and brine water volumes after mixing are not the same as when they were under initial condition. In order to solve this problem, the average-curvature equation is introduced.

$$H_a = \left|\frac{1}{R_o}\right| + \left|\frac{1}{R_w}\right| = \frac{1}{\xi^*} \quad (8)$$

$\xi^*$ is the characteristic length introduced by De Gennes and Taupin (1982). It is the maximum length scale at which any oil and brine water can be correlated to the surfactant membrane. It can be mathematically presented as Eq. 9a. However,

if the phase volumes data are not available, the characteristic lengths are calculated from the optimum solubilization ratio, Eq. 9b.

$$\xi^* = \frac{6C_O^m C_W^m V_m}{A_s} \tag{9a}$$

$$\xi^* = \frac{3\times\sigma^*\times MW\times 10^{24}}{a_s\times N_a} \tag{9b}$$

Where, $C_O^m$ is the volume fraction of oil in the middle phase microemulsion. $C_W^m$ is the volume fraction of brine water in the middle phase microemulsion. $V_m$ the is volume of the middle phase. $MW$ is the molecular weight of the surfactant or co-solvent. $\sigma^*$ is the optimum solubilization ratio. $a_s$ is the surface area per molecule of the surfactant or co-solvent; and $N_a$ is the Avogadro's number. The value of the characteristic length physically means the maximum solubilization capacity of a microemulsion system.

Once the values of $H_a$ and $\xi^*$ are determined, the types of systems can also be determined. When $1/H_a \leq \xi^*$, if $HLD \leq 0$, the system is a Type I system; if $HLD > 0$, the system is a Type II system. However, when $1/H_a > \xi^*$, the system falls into a Type III system (Acosta et al. 2012). $R_w$ and $R_o$ are calculated by solving net-curvature equation and average-curvature equation simultaneously. Hence, $R_w$ and $R_o$ are respectively given by,

$$R_w = \frac{2}{\left|\frac{1}{\xi^*}+\frac{HLD}{L}\right|} \tag{10}$$

$$R_o = \frac{2}{\left|\frac{1}{\xi^*}-\frac{HLD}{L}\right|} \tag{11}$$

Finally, by assuming the brine water density is equal to the surfactant density, which are equal to 1 g/mL; secondly and the volume of surfactant is

significantly smaller than the volume of brine water, the solubilization ratio of oil and brine water can be obtained respectively as,

$$\sigma_o = R_o \times \frac{A_s}{3V_w} \times \sum \frac{1}{C_{s_i}} \quad (12)$$

$$\sigma_w = R_w \times \frac{A_s}{3V_w} \times \sum \frac{1}{C_{s_i}} \quad (13)$$

Where, $\sigma_o$ is the solubilization ratio of oil. $\sigma_w$ is the solubilization ratio of brine water. $C_{s_i}$ is the concentration of each surfactant or co-solvent $i$. $R_O$ is the internal oil phase radius. $R_W$ is the internal brine water phase radius. $V_W$ is the volume of brine water in the system; and $A_s$ is the interfacial area provided by surfactant.

However, current HLD-NAC model has ignored the contributions of surfactant molecules to the micellar volume. This assumption is not valid when micelles are small. Surfactant volume becomes more significant as the size of micelles decreases (Khorsandi and Johns 2016). The drawbacks of current HLD-NAC model result in improvements of Eq. 5 and Eq. 6. A simple correction has been added in Eq. 5 and Eq. 6 by including the surfactant volumes in the micellar volume.

$$R_w = \frac{3 \times (V_w + V_s/2)}{A_s} \quad (14)$$

$$R_o = \frac{3 \times (V_o + V_s/2)}{A_s} \quad (15)$$

Where, $V_S$ is the surfactant volume. The ½ factor represents that half of the surfactant volume encompasses the micellar volume.

Additionally, engineers, who are modeling microemulsion phase behavior with HLD-NAC, need to be extremely careful of the units of every parameter. Since data of parameters could be recorded in different units, unit conversions

may create tremendous calculation burden so that occurrence of calculation errors may rise. To avoid the calculation inconvenience, Khorsandi and Johns (2016) transform the HLD-NAC model into dimensionless by using an $I-ratio$, which defined by Ghosh and Johns (2016), and the solubilization ratios.

The $I-ratio$ mathematical expression is given as,

$$I=\frac{V_s}{A_s L} \tag{16}$$

Where, $V_S$, $A_s$, and $L$ are defined as above. Recall $L$ is correlated to the surfactant tail length. Consequently, the $I-ratio$ is the ratio of the volume of a surfactant molecule in bulk phase to the volume of the same surfactant molecule in a micelle. The value of $I-ratio$ can be determined by matching experimental data even without a thorough understanding of the molecule structure. Therefore, finding the value of $I-ratio$ instead of conducting experiment to find the values of $a_{s_i}$, the surface area per molecule of the surfactant, is more convenient and practical when engineers perform HLD-NAC calculations. Eq. 14 and Eq. 15 can be reformed in term of $I-ratio$,

$$R_w=3IL(\sigma_w+0.5) \tag{17}$$

$$R_o=3IL(\sigma_o+0.5) \tag{18}$$

And then substitute Eq. 17 and Eq. 18 into HLD-NAC equations,

$$H_n=\frac{1}{\sigma_o+0.5}-\frac{1}{\sigma_w+0.5}=-3\times I\times HLD \tag{19}$$

$$H_a=\frac{1}{\sigma_o+0.5}+\frac{1}{\sigma_w+0.5}=\frac{6I}{\xi_D} \tag{20}$$

Where, $\xi_D=\xi/L$, which is the dimensionless characteristic length. For Type III systems, $\xi=\xi^*$, thus $\xi_D=\xi_D^*$.

If the system is a Type III system, which is at the optimum formulation. Combine Eq. 19 and Eq. 20, then the solubilization ratio at the optimum formulation can be computed as,

$$\sigma_O^* = 2[3I(H' - HLD)]^{-1} - 0.5 \quad (21a)$$

$$\sigma_w^* = 2[3I(H' + HLD)]^{-1} - 0.5 \quad (21b)$$

$$H' = 2/\xi_D^* \quad (22)$$

However, the contributions of co-solvents have not been well studied in published papers concerning the HLD-NAC model so far. Acosta et al. (2003) and Jin et al. (2015) assumed co-solvents were entirely adsorbed at the interface leading to underestimate the equivalent surfactant tail length. Therefore, improvements for the HLD-NAC model were desired, which will more physically represent the actual surfactant tail length.

### 2.2 Co-solvent (Alcohol) Partitioning

In order to have a better understanding of the effects of co-solvents on the HLD-NAC model when estimating phase behavior of chemical flooding, the co-solvent partitioning theory need to be reviewed. There are normally at least five components in chemical flooding. They are surfactants, co-solvents (typically alcohols), hydrocarbon, water and electrolytes. A strong phase behavior model should consider the effect of each component. However, many authors have reduced the number of actual components by combining similar components into pseudo-components for the mathematical simplicity of the phase behavior model. In chemical flooding simulations, oil is treated as one of the pseudo-components

(Salter 1978, Glinsmann 1979, Puerto and Reed 1983), while brine is the other one; and surfactant is the third one (Vinatieri and Fleming 1979). The overall compositions significantly affect the actual compositions of the pseudo-components. The actual compositions of the pseudo-components are a function of the overall compositions and are assumed independent of the salinity. For the purpose of simplicity, the slug composition is reduced to four pseudo-components: surfactant, co-solvent, oil and brine. In this study, co-solvents are considered to be alcohols.

The phase behavior of a four-component system was initially represented on three-dimensional quaternary diagrams in many studies (Salter 1978, Bellocq et al 1981, Blevins et al 1981). Later, researchers found that co-solvent can partition into all three phases in a Type III microemulsion system so that it was feasible to reduce diagram dimensionality (Salter 1978, Wickert et al 1978, Dominguez et al 1979, Blevins et al, 1981). This co-solvent distribution within every phase should result in phase compositions lying in the same ternary diagram where the overall composition point is also in the same diagram, shown in Figure 2. Hirasaki (1982) introduced the idea of fixed partition coefficients to associate the alcohol with the other components. Nevertheless, experimental results showed that the co-solvent partition coefficients varied with the overall compositions (Vinatieri and Fleming 1979, Dominguez et al. 1979, Wickert et al. 1979, Blevins et al, 1981). Biais et al. (1981) developed the pseudo-phase model, which was a thermodynamic model for co-solvent partitioning that can account for variable co-solvent partition coefficients. These pseudo-phases were not real phases but

pseudo-components which can be expressed on ternary diagrams. Their definitions will be discussed later in this study.

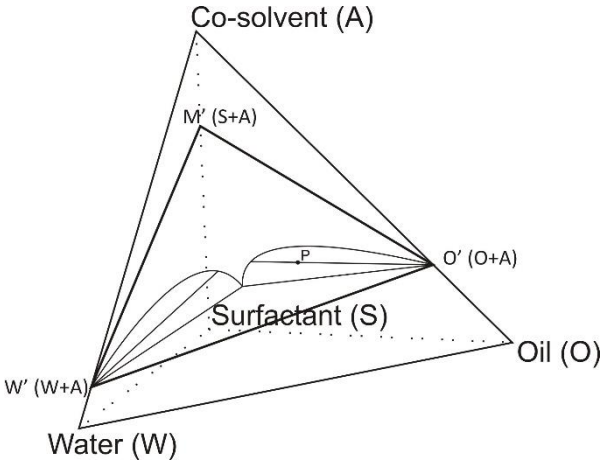


**Figure 2 Quaternary diagram in which are represented the volumetric compositions of microemulsions. Point P represents the overall compositions.**

### *2.2.1 Basic Assumption*

For the system consisting of two amphiphilic species ($A, S$), water with salt ($W$), and oil ($O$), brine and oil are pseudo-components, which behave as pure components do. For the purpose of modeling the partitioning, it is convenient to assume that a system had three pseudo-phases which are in thermodynamic equilibrium. The amphiphilic species $S$ is assumed to be in the interfacial pseudo-phase only, whereas amphiphilic species $A$ presents in each pseudo-phase. In a Type III system, the interfacial pseudo-phase ($M'$) separates the aqueous pseudo-phase ($W'$) and the oleic pseudo-phase ($O'$). The three pseudo-phases are defined as,

$Aqueous\ pseudo-phase\ (W') = brine + alcohol;$

$Oleic\ pseudo-phase\ (O') = oil + alcohol;$

$Interfacial\ pseudo-phase\ (M') = surfactant + alcohol.$

All pseudo-phases have equivalent chemical potentials, since they are in thermodynamic equilibrium. Equality of chemical potentials is expressed by two partition coefficients, which are independent of concentrations of the overall compositions but the temperature and system formulations. For monomeric alcohol within three pseudo-phases, the partition coefficients are defined as, $k_m$: the partition coefficient of monomeric alcohol between interfacial and oleic pseudo-phases; $k_w$: the partition coefficient of monomeric alcohol between aqueous and oleic pseudo-phases.

According to Gibb's phase rule, the aqueous excess phase has the same compositions as the aqueous pseudo-phase; and the oleic excess phase is identical to the oleic pseudo-phase. Thus, the $k_w$ and $k_m$ thermodynamic coefficients can adequately describe the tie lines of surfactant/co-solvent/oil/brine ternary systems.

### *2.2.2 Model of Co-solvent Partitioning*

There are four components in the overall mixture. They are brine ($W$), oil ($O$), surfactant ($S$), and alcohol ($A$). The equations to convert four components into three pseudo-components have been developed (Camilleri 1983).

$$\lambda = \frac{V_A^{W\prime}}{V_W} \tag{23}$$

$$\gamma = \frac{V_A^{O\prime}}{V_O} \tag{24}$$

$$\sigma = \frac{V_A^{M\prime}}{V_S} \tag{25}$$

Where, $V_W$, $V_O$, and $V_S$ are overall brine, oil, and surfactant volumes, respectively. $V_A^{W\prime}$, $V_A^{O\prime}$, and $V_A^{M\prime}$ represent the volume of association of alcohol to aqueous pseudo-phase, alcohol to oleic pseudo-phase, and alcohol to interfacial pseudo-phase, respectively. The associations of the alcohol within the interfacial, oleic, and aqueous pseudo-phases are described by fixed partition coefficients, which are ratios of the concentrations of two phases (Hirasaki 1982). The alcohol partition coefficients defined in Hirasaki's model then can be calculated by using the parameters above.

$$K_A^O = \frac{\gamma}{\lambda} \tag{26}$$

$$K_A^S = \frac{\sigma}{\lambda} \tag{27}$$

Later, Prouvost et al. (1985) developed a thermodynamic model accounting two monomeric alcohol reactions with the following thermodynamic constants:

$k_{w1}$: the partition coefficient of monomeric alcohol $A$ between aqueous and oleic pseudo-phases;

$k_{m1}$: the partition coefficient of monomeric alcohol $A$ between interfacial and oleic pseudo-phases;

$K_1$: self-association constant of monomeric alcohol $A$ in oleic pseudo-phase;

$a$: ratio of molar volume of monomeric alcohol $A$ to equivalent molar volume of surfactant;

$k_{w2}$, $k_{m2}$, $K_2$, $b$: similar coefficients for monomeric alcohol $B$. The model gives the following relationships:

$$V_A = \frac{k_{w1}\gamma_1[1+\gamma_1+\gamma_2(1+K_2)]V_W}{[1+\gamma_1(1+K_1)+\gamma_2][1+\gamma_1+\gamma_2(1+K_2-k_{w2})]-k_{w1}\gamma_1[1+\gamma_1+\gamma_2(1+K_2)]} + \gamma_1 V_O + \frac{ak_{m1}\gamma_1[1+\gamma_1+\gamma_2(1+K_2)]V_S}{[1+\gamma_1(1+K_1)+\gamma_2][1+\gamma_1+\gamma_2(1+K_2-k_{m2})]-k_{m1}\gamma_1[1+\gamma_1+\gamma_2(1+K_2)]} \quad (28)$$

$$V_B = \frac{k_{w2}\gamma_2[1+\gamma_1(1+K_1)+\gamma_2]V_W}{[1+\gamma_1+\gamma_2(1+K_2)][1+\gamma_1(1+K_1-k_{w1})+\gamma_2]-k_{w2}\gamma_2[1+\gamma_1(1+K_1)+\gamma_2]} + \gamma_2 V_O + \frac{bk_{m2}\gamma_2[1+\gamma_1(1+K_1)+\gamma_2]V_S}{[1+\gamma_1+\gamma_2(1+K_2)][1+\gamma_1(1+K_1-k_{m1})+\gamma_2]-k_{m2}\gamma_2[1+\gamma_1(1+K_1)+\gamma_2]} \quad (29)$$

Where, $V_A$ and $V_B$ are the overall volumes for alcohol $A$ and $B$, respectively. Eq. 28 and Eq. 29 have two unknowns, $\gamma_1$ and $\gamma_2$, and can be solved by the Newton Raphson iteration method. Then the intensive parameters (Eq. 23-25) can be calculated as following:

$$\lambda_1 = \frac{k_{w1}\gamma_1[1+\gamma_1+\gamma_2(1+K_2)]}{[1+\gamma_1(1+K_1)+\gamma_2][1+\gamma_1+\gamma_2(1+K_2-k_{w2})]-k_{w1}\gamma_1[1+\gamma_1+\gamma_2(1+K_2)} \quad (30)$$

$$\lambda_2 = \frac{k_{w2}\gamma_2[1+\gamma_1(1+K_1)+\gamma_2]}{[1+\gamma_1+\gamma_2(1+K_2)][1+\gamma_1(1+K_1-k_{w1})+\gamma_2]-k_{w2}\gamma_2[1+\gamma_1(1+K_1)+\gamma_2} \quad (31)$$

$$\sigma_1 = \frac{ak_{m1}\gamma_1[1+\gamma_1+\gamma_2(1+K_2)]}{[1+\gamma_1(1+K_1)+\gamma_2][1+\gamma_1+\gamma_2(1+K_2-k_{m2})]-k_{m1}\gamma_1[1+\gamma_1+\gamma_2(1+K_2} \quad (32)$$

$$\sigma_2 = \frac{bk_{m2}\gamma_2[1+\gamma_1(1+K_1)+\gamma_2]}{[1+\gamma_1+\gamma_2(1+\mathrm{K}_2)][1+\gamma_1(1+K_1-k_{m1})+\gamma_2]-k_{m2}\gamma_2[1+\gamma_1(1+K_1)+\gamma} \quad (33)$$

Finally, alcohol partition coefficients in a two-alcohol system can be calculated from Eq. 26 and Eq. 27,

$K_A^O = \frac{\gamma_1}{\lambda_1}, K_A^S = \frac{\sigma_1}{\lambda_1}$ for alcohol $A$;

$K_B^O = \frac{\gamma_2}{\lambda_2}, K_B^S = \frac{\sigma_2}{\lambda_2}$ for alcohol $B$.

When there is only one alcohol in the system, Eq. 28 can be reduced to a cubic equation:

$$A\gamma^3 + B\gamma^2 + C\gamma + D = 0 \tag{34}$$

Coefficients $A, B, C$ and $D$ can be calculated as below:

$$A = (1 + K - k_m)(1 + K - k_w) \tag{35}$$

$$B = k_w(1 + K - k_m)\frac{V_w}{V_O} + ak_m(1 + K - k_w)\frac{V_S}{V_O} - (1 - K - k_m)(1 + K - k_w)\frac{V_A}{V_O} + 2 + 2K - k_m - k_w \tag{36}$$

$$C = k_w\frac{V_W}{V_O} + ak_m\frac{V_S}{V_O} - (2 + 2K - k_m - k_w)\frac{V_A}{V_O} + 1 \tag{37}$$

$$D = -\frac{V_A}{V_O} \tag{38}$$

Then the partition coefficients are calculated as,

$$K_A^O = \frac{1+\gamma(1+K-k_w)}{k_w} \tag{39}$$

$$K_A^S = \frac{ak_m[1+\gamma(1+K-k_w)]}{k_w[1+\gamma(1+K-k_m)]} \tag{40}$$

The overall alcohol volumes can be obtained by volumetric balance,

$$V_A = \lambda_1 V_W + \gamma_1 V_O + \sigma_1 V_S \tag{41}$$

$$V_B = \lambda_2 V_W + \gamma_2 V_O + \sigma_2 V_S \tag{42}$$

where $V_W$, $V_O$, $V_S$, $V_A$, $and\ V_B$ are the volumes of each overall compositions considering a two-alcohol system. Substitute $K_A^O$, $K_A^S$, $K_B^O$ and $K_B^S$ for $\gamma_1$, $\sigma_1$, $\gamma_2$ and $\sigma_2$ in Eq. 41 and Eq. 42,

$$V_A = \lambda_1 V_W + \lambda_1 K_A^O V_O + \lambda_1 K_A^S V_S \quad (43)$$

$$V_B = \lambda_2 V_W + \lambda_2 K_B^O V_O + \lambda_2 K_B^S V_S \quad (44)$$

Then $\lambda_1$ and $\lambda_2$ are calculated as following,

$$\lambda_1 = \frac{V_A}{(V_W + K_A^O V_O + K_A^S V_S)} \quad (45)$$

$$\lambda_2 = \frac{V_B}{(V_W + K_B^O V_O + K_B^S V_S)} \quad (46)$$

Finally, the volume fractions of each pseudo-component ($V_{PW}$, $V_{PO}$, $V_{PS}$) representing the apexes of a ternary diagram can be calculated as,

$V_{PW}$ =(brine volume)+(alcohol volume associated with brine)

$$V_{PW} = V_W + \lambda_1 V_W + \lambda_2 V_W$$

$$V_{PW} = V_W(1 + \lambda_1 + \lambda_2) \quad (47)$$

$V_{PO}$ =(oil volume)+(alcohol volume associated with oil)

$$V_{PO} = V_O + \gamma_1 V_O + \gamma_2 V_O$$

$$V_{PO} = V_O(1 + \lambda_1 K_A^O + \lambda_2 K_B^O) \quad (48)$$

$V_{PS}$ =(surfactant volume)+(alcohol volume associated with surfactant)

$$V_{PS} = V_S + \sigma_1 V_S + \sigma_2 V_S$$

$$V_{PS} = V_S(1 + \lambda_1 K_A^S + \lambda_2 K_B^S) \quad (49)$$

# Chapter 3: Methodology

## 3.1 HLD-NAC with Co-solvent Partitioning Algorithm

An algorithm was developed based on the HLD-NAC EOS coupled with the Biais' and Hirasaki's model to consider the partitioning of the co-solvent. Following the algorithm as presented in Figure 3, obtained or calculated the alcohol partition coefficients $K_A^O$ and $K_A^S$ as well as the properties of the surfactant and oil in the system, and droplet sizes of micelles were computed. Finally, the phase type can be determined. It presented an improved model which can more physically represent the actual surfactant tail length. The flow chart for solubilization ratio and IFT estimation by the HLD-NAC model coupled with the co-solvent partitioning model was presented in Figure 3. For the most part, there were one group of input parameters for the co-solvent partitioning model and, three groups of input parameters for the HLD-NAC model:

(1) The co-solvent (alcohol) partition coefficients $K_A^O$ and $K_A^S$;

(2) Properties of the surfactants and oils such as $Cc$, $K$, $EACN$, $a_s$ and $L$, etc.;

(3) Experimental data including volume fractions of brine water, oil and surfactants, salinity, temperature and pressure;

(4) Optimum salinity $S^*$ and the characteristic length $\xi^*$ at formulation design conditions from phase behavior test results.

The general assumptions in the algorithm were also listed by Jin et al. (2015) and were listed as follows:

(1) Microemulsion could be represented as coexisting hypothetical spherical droplets of oil and brine water;

(2) The surfactant concentration in the monomer form is negligible;

(3) Surfactant head area is constant at different salinities;

(4) Surfactant density is 1 g/mL in calculating surfactant mole concentration;

(5) Pseudo-components are the oleic, aqueous and the interfacial pseudo-phases.

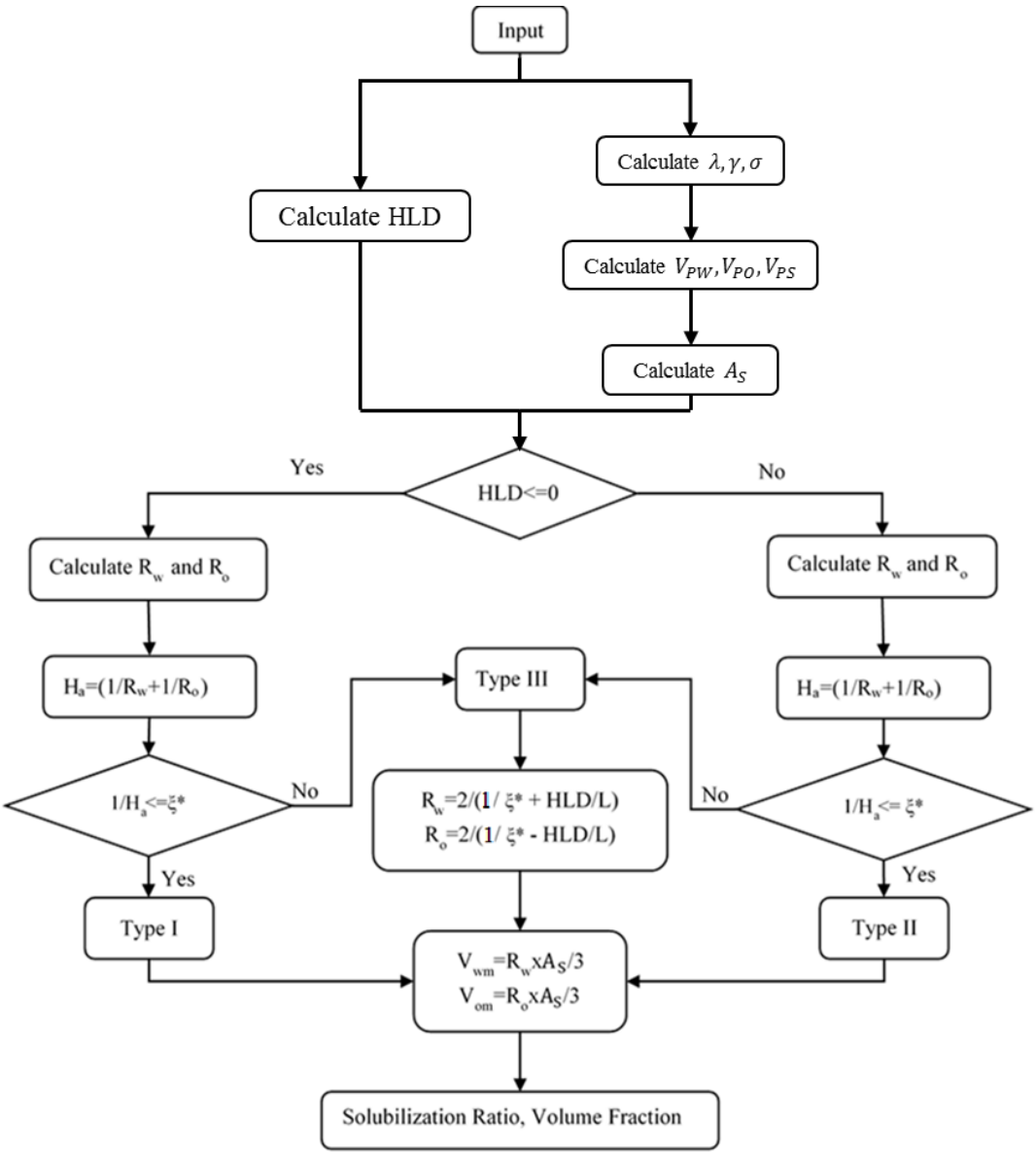


**Figure 3 Flow chart of HLD-NAC model coupled with the co-solvent partitioning**

Five microemulsion systems were used to examine the developed approach. In order to do so, solubilization ratios under salinity scan of these systems were reproduced by the HLD-NAC model coupled with the co-solvent partitioning mode.

### 3.2 Experimental Measurements

Table 1 summarized the properties of oils and surrogate oils (a mixture of dead crude and a pure hydrocarbon) used in this study.

**Table 1 Oil properties**

| Oil | Temperature (°C) | API | EACN |
|---|---|---|---|
| A | 38 | 45.4 | 10 |
| B | 38 | 45.4 | 16 |
| C | 85 | 37 | 10 |
| D | 85 | 29 | 13.45 |

This study used the microemulsion phase behavior methodology to evaluate the surfactant and co-solvent formulations listed in Table 2. Comprehensive experimental procedures can be found in Levitt et al. (2009), Lu et al. (2014a 2014b, and 2014c) and Chang et al. (2016). The selected surfactant formulations displayed ultralow IFT and formed low-viscosities microemulsions after cautious observation for a prolonged period of time.

A set of surfactants and co-solvents head area data from various literatures was used in this study. The surfactant area per surfactant molecule at the interface was calculated by the slope of the straight line in the semi-log plot of surface tension against logarithm of surfactant concentration, when the surfactant concentration was lower but close enough to the Critical Micelle Concentration (CMC). The surface concentration reached a constant maximum value and the interface was considered to be saturated with the surfactant at CMC (Rosen, 2004).

The properties of surfactants and co-solvents were listed in Table 2. The guerbet alkoxy carboxylates (GAC) and internal olefin sulfonates (IOS) surfactants were measured with the presence of 2 wt% NaCl addition at room

temperature and were taken from Rosen (2004). PO-sulfates and co-solvents properties were approximated to those with similar structures (Rosen, 2004).

**Table 2 Properties of surfactants and co-solvents**

| Descriptive name | Abbreviated chemical formula | MW (g/mole) | Head area $a_s$, (Å$^2$) |
|---|---|---|---|
| $C_{15-18}$ internal olefin sulfonate (IOS) | $R-CH(OH)-CH_2-CH(SO_3^-)-R'$, $R'-CH=CH-CH(SO_3^-)-R'$ Where $R+R'=C_{12}-C_{15}$ | 326 | 56 [a] |
| $C_{19-23}$ internal olefin sulfonate (IOS) | $R-CH(OH)-CH_2-CH(SO_3^-)-R'$, $R'-CH=CH-CH(SO_3^-)-R'$ Where $R+R'=C_{16}-C_{20}$ | 398 | 50 [a] |
| $C_{20-24}$ internal olefin sulfonate (IOS) | $R-CH(OH)-CH_2-CH(SO_3^-)-R'$, $R'-CH=CH-CH(SO_3^-)-R'$ Where $R+R'=C_{17}-C_{21}$ | 410 | 51 [a] |
| $C_{18}-45PO-30EO-$carboxylate | $R,R'-O-(CH_2-CH(CH_3)-O)_{25}-(CH_2-CH_2-O)_{25}-CH_2-CO_2^-$ Where $R+R'=C_{28}$ Where $R+R'=C_{17-21}$ | 4206 | 194 [a] |
| $C_{28}-25PO-25EO-$carboxylate | $R,R'-O-(CH_2-CH(CH_3)-O)_{25}-(CH_2-CH_2-O)_{25}-CH_2-CO_2^-$ Where $R+R'=C_{28}$ Where $R+R'=C_{17-21}$ | 3011 | 170 [a] |
| $C_{13}-13PO-$ sulfate | $C_{13}-O-(CH_2(CH_3)CH-O)_{13}-SO_3^-$ | 1041 | 60 [b] |
| $C_{16-17}-7PO-$ sulfate | $C_{16-17}-O-(CH_2(CH_3)CH-O)_7-SO_3^-$ | 741 | 60 [b] |
| Phenol $-$ 2EO | $(CH)_5-C-(CH_2-CH_2-O)_2-OH$ | 182 | 40 [b] |
| Phenol $-$ 4EO | $(CH)_5-C-(CH_2-CH_2-O)_4-OH$ | 270 | 40 [b] |
| $sec-$ Butanol (SBA) | $CH_3CH_2CH(OH)CH_3$ | 74 | 30 [b] |
| $iso-$ Butanol (IBA) | $(CH_3)_2CHCH_2OH$ | 74 | 30 [b] |

a: Lab measured at 2 wt% NaCl, room temperature

b: Obtained from reference (Rosen 2004)

## 3.3 Methods for Modeling Binodal Curve

The improved HLD-NAC model discussed earlier can be used to plot the binodal curves in ternary diagrams. Number of phases and the concentrations of compositions in microemulsion phase are determined with plotted ternary diagrams. Therefore, binodal curves with high accuracy are essential to the formulation designs for surfactant/alcohol mixtures.

A binodal curve separates the single-phase and two-phase regions in a ternary diagram. Above the binodal curve is a single-phase region, while below the curve is a two-phase region (Sheng 2010). The concentrations of each composition in microemulsion phase lie on the binodal curve. Binodal curves are determined by the solubilization ratios either obtained from experimental data or calculated from the HLD-NAC model. Engineers can graphically predict the concentrations of compositions in microemulsion phase with the accurate binodal curves in ternary diagrams.

### *3.3.1 Catastrophic Phase Inversion Theory*

Jin et al. (2016a) has applied the catastrophic phase inversion theory to the HLD-NAC model so that the model was applicable to various oil-brine ratios and surfactant concentrations. The HLD-NAC model can plot a system with known overall compositions on the ternary phase diagrams with oil, brine water and surfactant as the pseudo-components. Catastrophic phase inversion theory, which indicated that when the internal phase volume fraction in the microemulsion increased to some point, the internal phase inversed to the external phase, was

feasible to locate the plait points on ternary diagrams (Salager et al. 1983). This approach assumes that the solubilization ratio is constant under a particular salinity so that the line, which is connecting one lower apex of ternary diagram and the concentration point of the composition in microemulsion phase after the system reached equilibrium, forms one part of the binodal curve. Catastrophic phase inversion is assumed to occur in the single phase when internal phase volume fraction is over than 75% (Salager et al. 1983, Salager et al. 2000b, Salager et al. 2001). Thus, another line, which is connecting the upper apex and 75% point for Type I systems or 25% point for Type II systems on the lower axis of the ternary diagram, can be determined. The interception of these two lines is the plait point, where all compositions are the same. The binodal curve is finally completed by connecting the plait point and the other lower apex (Jin et al. 2016a). The binodal curve plotted by this mothed shows a sharp triangle multiphase region, shown as Figure 4. Ideally, the real system which has more gradual transition near plait point should be included in the sharp triangle region.

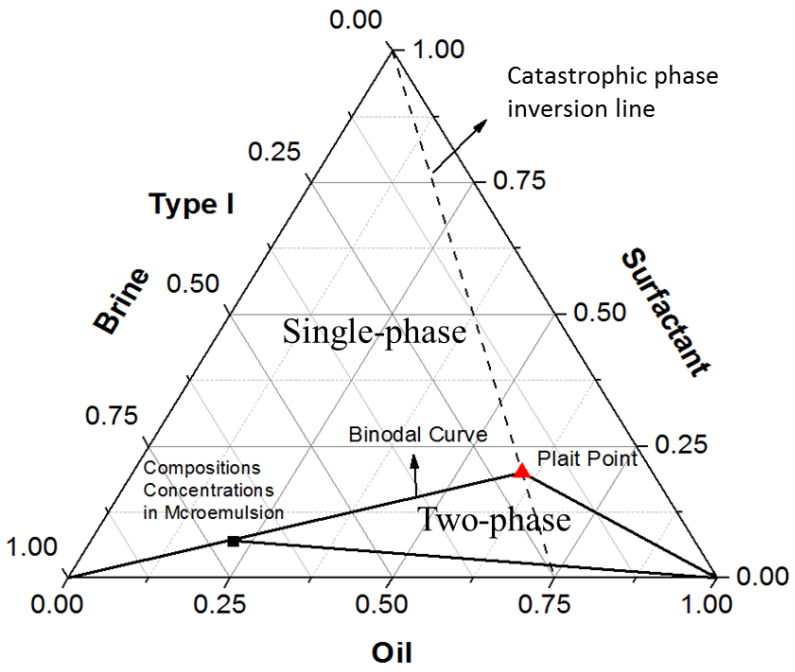


**Figure 4 Binodal curve made by catastrophic theory (Jin et al. 2016b)**

However, sharp angle means that the model is discontinuous; and the discontinuities can create significant errors in many applications, especially when performing numerical simulation.

### *3.3.2 Khorsandi and Johns' Flash Algorithm*

In order to create a smooth binodal curve which can represent the real system, a different algorithm based on the dimensionless HLD-NAC model discussed in Chapter 2 was developed by Khorsandi and Johns (2016) to eliminate the use of catastrophic theory. This algorithm has created the smooth binodal curves in every Winsor type system and successfully matched experimental data.

This flash algorithm was developed from the observation which the binodal curve originated from the point of tangency of a tie line and itself, and ended at the interception point of another tie line of itself. The binodal curve can

be found by an algorithm which is dependent on the interpolation on tie line functions. The functions of the two tie lines at each end of the binodal curve need to be determined before the interpolation. One is the limiting tie line which is tangent to the binodal curve; while the other one is the tie line that forms one of the boundaries of the three-phase tie triangle. Inside the three-phase tie triangle is the three-phase region. Therefore, tie line functions need to be determined prior to the performance of this flash algorithm.

#### *3.3.2.1 Tie Line*

Tie lines are the lines that connecting two equilibrium phases. Since HLD-NAC model assumes that the excess phase is either complete oil or brine water, tie lines always emanate from the oil apex or brine water apex. All possible proportions of the two phases could be found along the tie lines. In Type I systems, the function of tie line is,

$$V_S = a_- V_W + b_- \tag{50}$$

$$a_- = -\frac{1}{1+\sigma_w^i} \tag{51}$$

$$b_- = -a_- \tag{52}$$

For Type II systems,

$$V_S = a_+ V_O + b_+ \tag{53}$$

$$a_+ = -\frac{1}{1+\sigma_O^i} \tag{54}$$

$$b_+ = -a_+ \tag{55}$$

From Eq. 50 to Eq. 55, $a$ is the slope of tie line, and $b$ is the interception of the tie line with the axis of the ternary diagram. The interception point is on the

axis where either oil overall composition is zero for Type I systems or brine water overall composition is zero for Type II systems.

*3.3.2.2 Determine the Starting Point and the Endpoint of Binodal Curve*

The binodal curve starts from the point of tangency of a tie line and itself. The binodal curve separates single-phase and two-phase regions in a ternary diagram. Above the binodal curve is the single-phase region, while below the curve is the two-phase region. Compositions in microemulsion phase reach equilibrium along the binodal curve. Because of the assumption that excess phase is either complete oil or complete brine water, the point of tangency must be either the oil apex or the brine water apex of the ternary diagram. Therefore, the starting point of binodal curve is one of the lower apexes. The starting point is the oil apex in a Type I system, whereas in a Type II system, the starting point is the brine water apex. The tie line tangents to the binodal curve is called limiting tie line. It represents the condition that there is only one phase existing so that the limiting tie line is tangent to the two-phase region. Under such condition, Eq. 20 becomes,

$$\frac{1}{0.5+\sigma_j^c} = \frac{6I}{\xi_D^c}, j = w, o \tag{56}$$

For a Type I system, $j$ is $w$, representing the component in the microemulsion is brine and the characteristic length is $\xi_{D-}^c$. For a Type II system, $j$ is $o$, meaning the component is oil and the characteristic length is $\xi_{D+}^c$. The superscript $c$ means limiting condition. The value of $\sigma_j^c$ could be positive or negative. A positive value means that the limiting tie line is in the ternary diagram, and that the starting point

of binodal curve is the lower apex. However, the limiting tie line will be at the outside of the ternary diagram if the value of $\sigma_j^c$ is negative. Therefore, the point of tangency could be not in the ternary diagram, and then the starting point is the cross point of the binodal curve and the axis of the ternary diagram as shown in Figure 5.

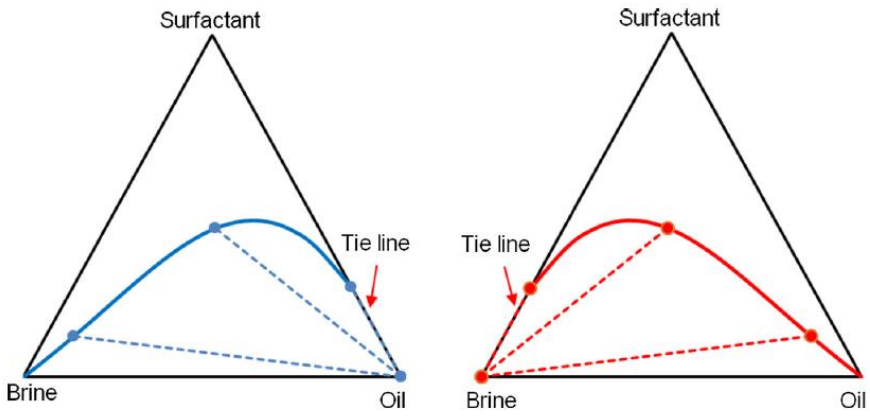


**Figure 5 The limiting tie line is not inside the ternary diagram (Khorsandi and Johns 2016)**

The binodal curve will end once it reaches the tie triangle which representing the boundary of three-phase region. The boundary of the tie triangle could be either inside or outside the ternary diagrams depending on the system salinity, shown as Figure 6 and Figure 7. If there is no three-phase region in the ternary diagram, which meaning the system is either Type I or Type II system, the boundary of the tie triangle is outside the ternary diagram. The binodal curve will go through the lower apex of ternary diagram and continuously go beyond until it arrives at the boundary of tie triangle. However, the portion beyond the apex of the binodal curve has no significant function for predicting the system

composition. It is only for interpolation. The boundaries of the tie triangle are mathematically given as,

$$V_S = a_-^* V_W + b_-^* \tag{57a}$$

$$V_S = a_+^* V_O + b_+^* \tag{57b}$$

Eq. 57a and Eq. 54b represent the right boundary and the left boundary of the tie triangle, respectively.

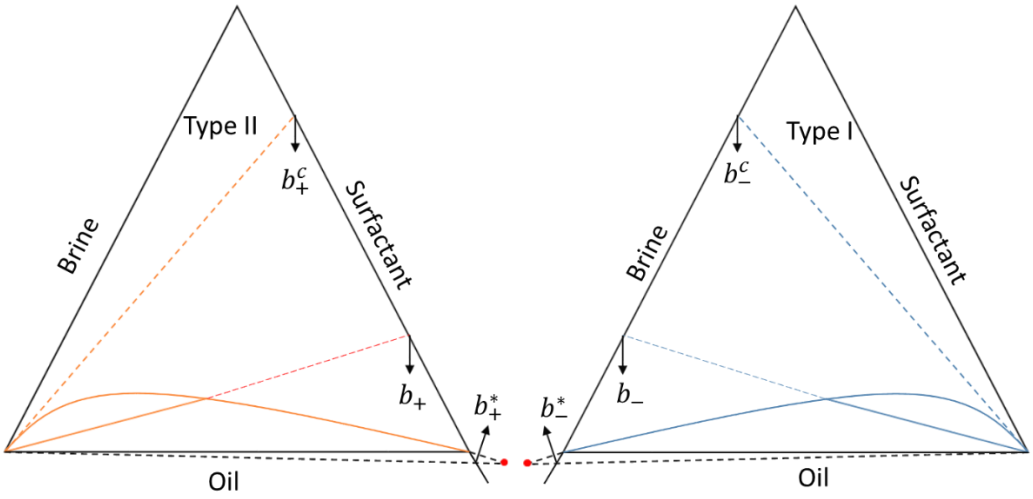


**Figure 6 The boundary of tie triangle is outside the ternary diagram (Khorsandi and Johns 2016)**

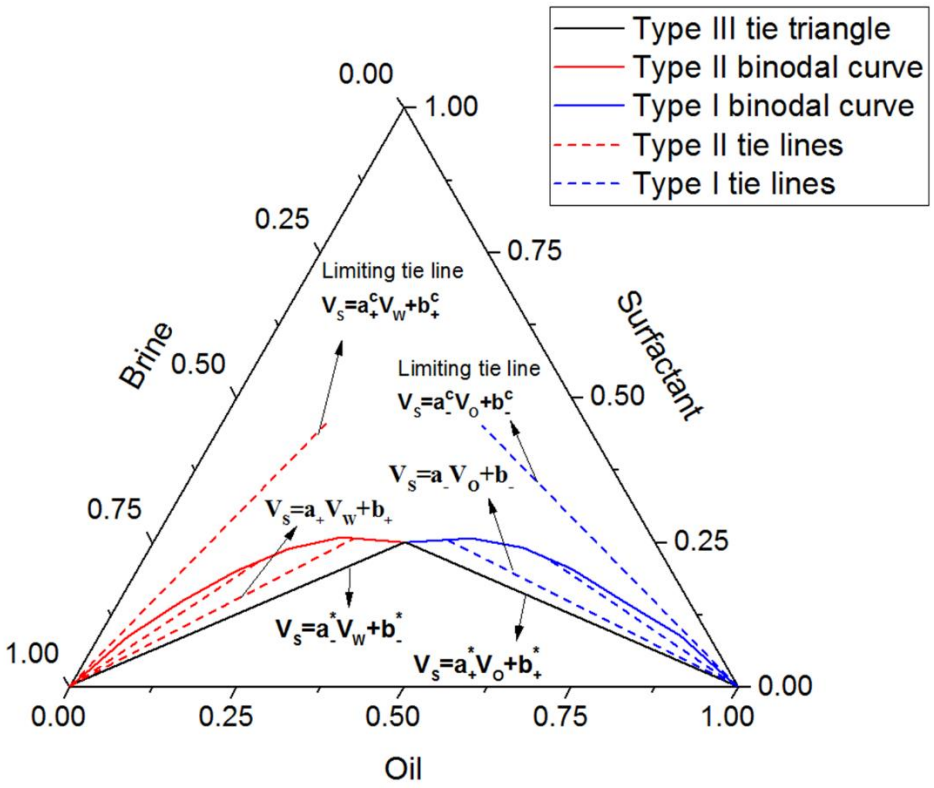


**Figure 7 The boundary of tie triangle is inside the ternary diagram (Khorsandi and Johns 2016)**

*3.3.2.3 Determine the Characteristic Length*

Inspect Eq.51 (or Eq. 54) and Eq. 56, the slope of tie line is a function of the characteristic length. Each tie line has one associated value of characteristic length. The characteristic length related to the limiting tie line for a Type I system can be calculated as,

$$\frac{1}{\xi_{D-}^c} = C_1\left(1 - e^{C_2(HLD-H')}\right) + \frac{1}{\xi_D^*} \tag{58}$$

Where, $C_1$ and $C_2$ are the fitting parameters based on available data. The same equation can be used to find $\xi_{D+}^*$ by tuning $C_1$ and $C_2$ with Type II systems experimental data.

The characteristic lengths in the two-phase region are calculated by using linear interpolation. For a Type I system,

$$\frac{1}{\xi_D} = \frac{1}{\xi_{D-}^c} - A_-(b_-^c - b_-) \tag{59}$$

$$\text{where, } A_- = \left(\frac{1}{\xi_{D-}^c} - \frac{1}{\xi_D^*}\right) \Big/ (b_-^c - b_-^*) \tag{60}$$

$$b_-^* = \frac{1}{1+\sigma_W^*} \tag{61}$$

$$b_-^c = \frac{1}{1+\sigma_W^c} \tag{62}$$

Similar equations can be used to find the characteristic lengths for the Type II systems.

However, there are no studies in published papers accounting the contributions of alcohol for the Khorsandi and Johns' model and algorithm. Thus, significant errors may occur when engineers use this model to design the surfactant/alcohol EOR process. This study presented a new algorithm which coupling the Khorsandi and Johns' flash algorithm with the thermodynamic-based co-solvent phase partitioning model.

#### *3.3.2.4 Tuning for $C_1$ and $C_2$*

The purpose of tuning is not only to provide a good fit to experimental data, but also to generate an accurate model to predict the number of phases and types of phases and their compositions without doing any experiment so that cost can be reduced. The coefficients of the model for the characteristic lengths associated with limiting tie lines can be adjusted by matching the available two-

phase region data. It is worth noting that each Winsor type system can have its own values of $C_1$ and $C_2$. In other word, it is not necessary that there are universal $C_1$ and $C_2$ good for all Winsor type systems. Further, in the Type III system, $C_1$ and $C_2$ are different between left lobe and right lobe.

The experimental data should be sufficient in ensuring that the estimated fitting parameters will not create significant errors or underestimate the solubilization capability of the system. General tuning process is that initial guesses of $C_1$ and $C_2$ are made first; and then, based on the experimental data plotted on the ternary diagram, adjust the initial guesses to minimize the mean square error between experimental data and predicted values.

### *3.3.3 Khorsandi and Johns' Flash Algorithm with Co-solvent Partitioning Model*

A new algorithm was developed based on Khorsandi and Johns' flash algorithm coupled with the Biais' and Hirasaki's model to consider the partitioning of the co-solvent.

#### *3.3.3.1 Flow Chart*

Once the tie line functions and the values of characteristic lengths are determined, the new algorithm methodology for all Winsor types can be outlined. Figure 8 showed a flow chart for this algorithm

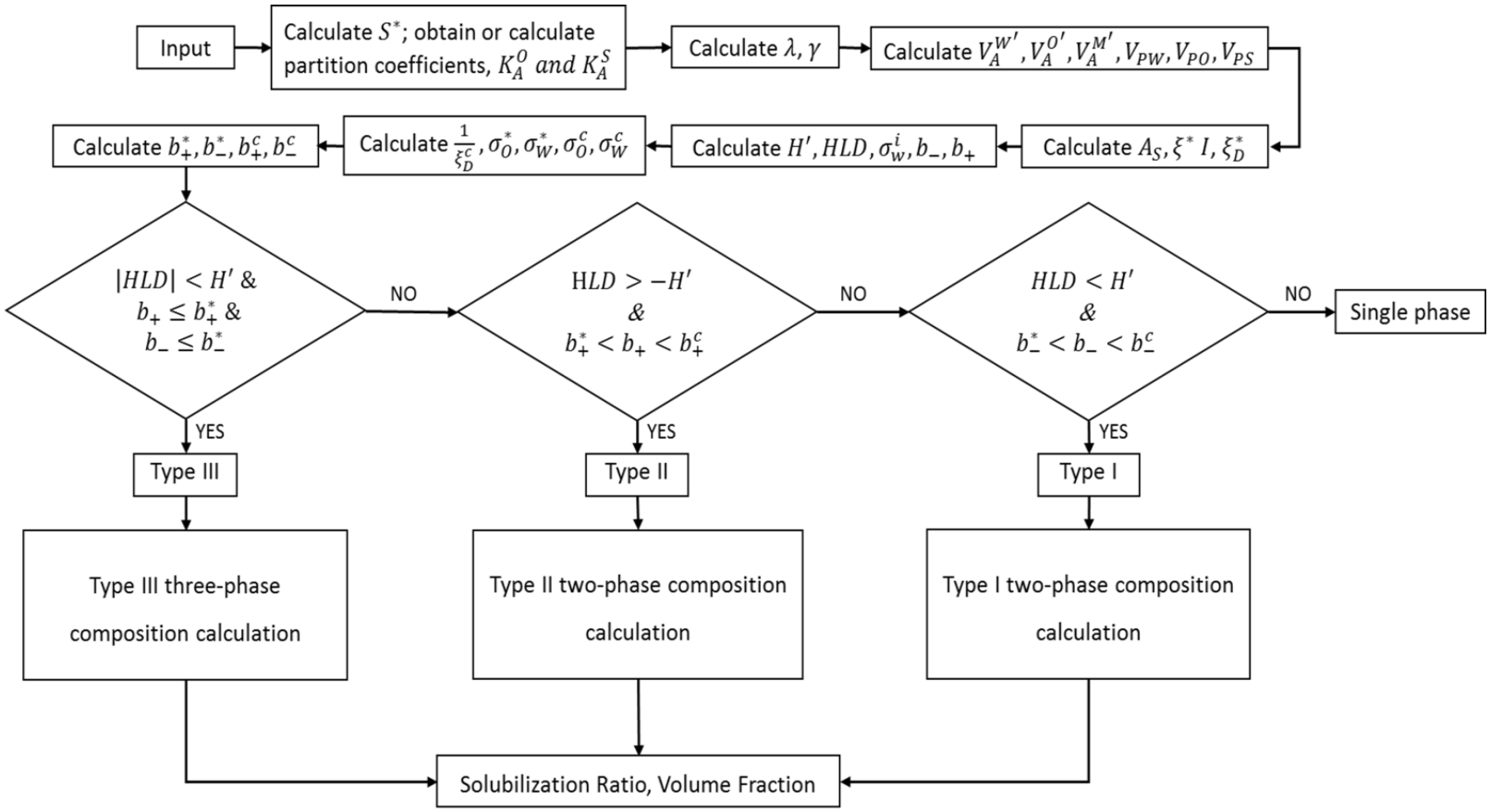


**Figure 8 Flow chart for the algorithm coupling the original Khorsandi and Johns' flash algorithm with the thermodynamic-based co-solvent partitioning model**

The new algorithm also starts with one group of input parameters for the co-solvent partitioning model, and three groups of input parameters for the HLD-NAC model:

(1) The co-solvent (alcohol) partition coefficients $K_A^O$ and $K_A^S$;

(2) Properties of the surfactant and oil such as $Cc, K, EACN, \alpha\ and\ L$, etc.;

(3) Experimental data including salinity, temperature, pressure, and volume fractions of water, oil and surfactants;

(4) Optimum salinity $S^*$ and the characteristic length $\xi^*$ at formulation design conditions from phase behavior test results.

With the input parameters, the interception points of ternary diagram axes and each boundary tie line of the tie triangle can be calculated even though there is no three-region in the ternary diagram. These values of the interception points are used for interpolation of the characteristic lengths in the two-phase region only. The limiting tie lines for their corresponding two-phase regions can also be inside or outside the ternary diagram, but they are always used for the purpose of interpolation.

Interception points are useful for estimating that whether an overall composition point is within the three-phase region. If the condition below is held,

$$|HLD| < H'\ and\ b_- \le b_-^*\ and\ b_+ \le b_+^* \tag{63}$$

the overall composition is in three-phase region. The system is a Type III system. The algorithm goes to three-phase composition calculations, which are given by,

$$C_S^M = 1/(1 + \sigma_O^* + \sigma_W^*) \tag{64}$$

$$C_W^M = C_S^M \times \sigma_W^* \tag{65}$$

$$C_O^M = 1 - C_S^M - C_W^M \quad (66)$$

Where, $C_S^M$ is the volume fraction of surfactant in middle phase microemulsion. $C_W^M$ is the volume fraction of water in middle phase microemulsion. And $C_O^M$ is the volume fraction of oil in middle phase microemulsion.

If Eq. 63 is not true, the system could be in Type II region. The following condition should be examined,

$$HLD > H' \; and \; b_+^* < b_+ \leq b_+^c \quad (67)$$

When Eq. 67 is true, the system is a Type II system. Two-phase composition calculations should be performed at this time. Solubilization ratio for brine water in microemulsion phase need to be determined, which is followed by the calculations of volume fractions for each component in miroemulsion phase. The brine water solubilization ratio is given as,

$$\frac{1}{\sigma_W + 0.5} = \frac{6I}{\xi_D} - \frac{1}{\sigma_O^i + 0.5} \quad (68)$$

Once the solubilizaion ratio is determined, volume fractions of each component in microemulsion phase can be calculated as,

$$C_S^M = 1/(1 + \sigma_O^i + \sigma_W) \quad (69)$$

$$C_W^M = C_S^M \times \sigma_W \quad (70)$$

$$C_O^M = 1 - C_S^M - C_W^M \quad (71)$$

If Eq. 67 is not true either, the system could be either in Type I region or in single phase region. To determine which regions the system is actually in, the following condition could be used to check,

$$HLD < H' \; and \; b_-^* < b_- < b_-^c \quad (72)$$

The system is in Type I region when this condition is satisfied. Since the excessive phase is brine water in this region, the oil solubilization ratio in microemulsion phase need to be calculated first; and then the volume fractions of each component in the microemulsion phase can be determined. The oil solubilizaiton ratio is given as,

$$\frac{1}{\sigma_O+0.5} = \frac{6I}{\xi_D} - \frac{1}{\sigma_W^i+0.5} \tag{73}$$

the volume fractions of each component in microemulsion phase can be calculated as,

$$C_S^M = 1/(1+\sigma_W^i+\sigma_O) \tag{74}$$

$$C_O^M = C_S^M \times \sigma_O \tag{75}$$

$$C_W^M = 1 - C_S^M - C_O^M \tag{76}$$

If none of the conditions (Eq. 63, Eq. 67 and Eq. 72) is held, the system is a single-phase system. An example is shown in the results section to demonstrate this new algorithm.

# Chapter 4: Results and Discussions

## 4.1 Determination of Length Parameter

In order to validate the HLD–NAC model coupled with the co-solvent partitioning model for microemulsion systems with crude oil, solubilization ratio curves were simulated for formulations with various surfactant mixtures, co-solvents as well as oils.

Because of the synergistic enhancement effects, most of the formulations for surfactant flooding are mixtures. In this section, solubilization ratio curves of surfactant mixtures and crude oils along with the co-solvents were reproduced by the HLD–NAC model coupled with the co-solvent partitioning model. GAC surfactants used in this section were synthesized at the University of Texas at Austin, and had shown excellent performance under harsh reservoir conditions like high salinity, high hardness and high temperature (Lu et al. 2014a). Phase behavior experimental data in this section were lab measured.

Table 3 showed the alcohol partition coefficients for the five formulations used in this study. For formulations 1,2 and 3, the oil-brine partition coefficients ($K_A^O$) were calculated from Dwarakanath and Pope (1998) correlation, which related the alcohol EACN and the oil EACN, shown as Eq. 77.

$$\log(K_A^O) = -2.9562 + 0.6548 \times EACN_{alcohol} - 0.0505 \times EACN_{oil} \qquad (77)$$

Brine-interfacial pseudo-phase partition coefficients ($K_A^S$) were assumed based on the length parameters calculated from Acosta et al. (2003) and Acosta (2008). Partition coefficients for Formulations 4 and 5 in Table 3 were taken from Chang et al. (2016).

**Table 3 Simulated formulation summary**

| No. | Surfactant formulations | Oil | Optimum salinity $S^*$, ppm | Optimum sol. ratio, $\sigma$, cc/cc | Alcohol at the interfacial phase, wt% | Alcohol partition coefficients | | Characteristic length, $\xi^*$, Å | | Length parameter, L, Å | |
|---|---|---|---|---|---|---|---|---|---|---|---|
| | | | | | | $K_A^O$ | $K_A^S$ | Co-solvent partition? | | | |
| | | | | | | | | Yes | No | Yes | No |
| 1 [a] | 0.75 wt% of $C_{16-17} - 7PO - sulfate$, 0.25 wt% of $C_{15-18} - IOS$, and 2.0 wt% SBA | A | 41,000 | 12 | 0.323 | 0.20 * | 11 ** | 254.6 | 57 | 24 | 5 |
| 2 [b] | 1.5 wt% of $C_{16-17} - 7PO - sulfate$, 0.5 wt% of $C_{20-24} - AOS$, and 4.0 wt% SBA | A | 17,000 | 11 | 1.231 | 0.20 * | 12 ** | 157 | 50 | 28 | 8 |
| 3 [b] | 0.5 wt% of $C_{13} - 13PO - sulfate$, 0.5 wt% of $C_{20-24} - IOS$, and 2.0 wt% IBA | B | 21,000 | 20 | 0.311 | 0.15 * | 10 ** | 459.2 | 100 | 35 | 8 |
| 4 [c] | 0.66 wt% of $C_{28}(O) - 25PO - 25EO - COO$, 0.3 wt% of $C_{15-18} - IOS$, 0.4 wt% of $C_{19-23} - IOS$ and 0.6 wt% Phenol − 4EO | C | 57,000 | 8.5 | 0.045 | 0.58 | 7.72 | 395.1 | 252.7 | 40 | 20 |
| 5 [c] | 0.4 wt% of $C_{18} - 45PO - 30EO - COO$, 0.6 wt% of $C_{19-23} - IOS$, and 0.5 wt% of Phenol − 2EO | D | 30,000 | 11 | 0.084 | 0.55 | 13.04 | 488.5 | 269.1 | 60 | 40 |

a: From reference (Lu et al. 2014b); b: From reference (Levitt et al. 2009); c: From reference (Chang et al. 2016)

*: Calculated value according to Dwarakanath and Pope (1998); **: Estimation made according to Acosta et al. (2003)

Five solubilization ratio curves and phase volume fraction diagrams of single surfactant and surfactant mixtures with alcohols as co-solvents for various crude oils were modeled. Figure 9 to Figure 13 showed the matched solubilization ratio with different formulations.

Figure 9 presented phase behavior results of a 0.75 wt% of $C_{16} - 17 - 7PO - sulfate$, 0.25 wt% of $C_{15} - 18 - IOS$, and 2.0 wt% $SBA$ for Oil A. The optimum salinity was observed at 41,000 ppm. All parameters were shown as Formulation 1 in Table 3. When all alcohol, 2.0 wt%, was assumed to partition onto the interface, the interfacial area was large and the estimated characteristic length ($\xi^*$) of 57 Å from Eq. 9a as well as the matched length parameter ($L$) of 5 Å were relatively low, due to the dependence of fitting the solubilization ratio of Type I and Type II systems on both the interfacial area ($A_s$) and the length parameter. However, the alcohol partitioning within three phases led to a more physical representation of the characteristic length of 254.6 Å and a length parameter of 24 Å. The estimated alcohol volume partitioning into the interfacial pseudo-phase from Eq. 49 was 0.323 wt%.

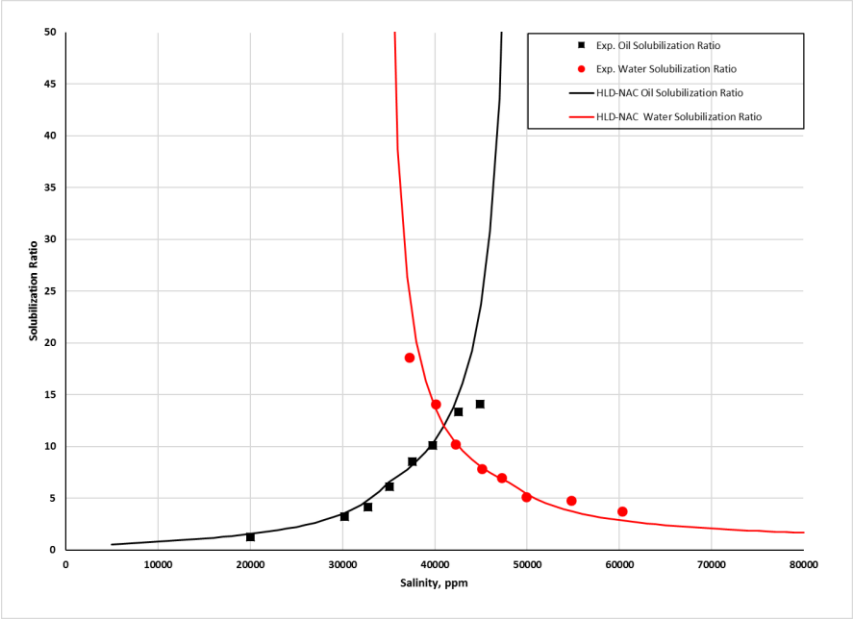


**Figure 9 HLD-NAC modeled phase behavior of a 0.75 wt% of $C_{16–17}$−7PO−sulfate, 0.25 wt% of $C_{15–18}$−IOS, and 2.0 wt% SBA for Oil A**

Figure 10 and Figure 11 presented the experimental data from Levitt et al. (2009) and the solubilization ratio curves calculated by the HLD-NAC model coupled with the co-solvent partitioning model. All parameters were shown as Formulation 2 and Formulation 3 in Table 3. Optimum salinity for Formulation 2 system was 17,000 ppm, while for Formulation 3 was 21,000 ppm. The calculated characteristic length and the matched length parameter under the co-solvent partitioning model for Formulation 2 were 157 Å and 28 Å, respectively. For Formulation 3, the characteristic length and the length parameter were 459.2 Å and 100 Å, respectively. The alcohol volume in the interfacial pseudo-phase was 1.231 wt% for Formulation 2, while 0.311 wt% for Formulation 3.

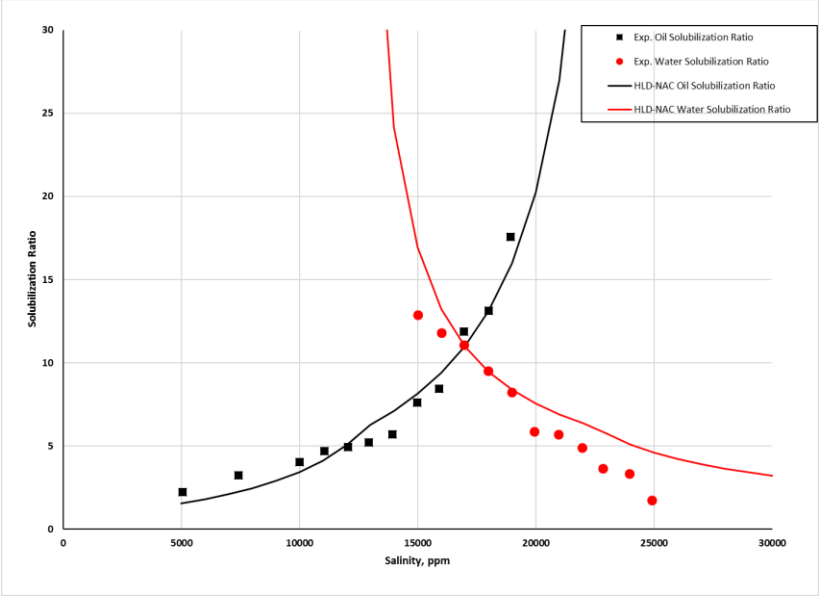


**Figure 10 HLD-NAC modeled phase behavior of a 1.5 wt% of $C_{16\text{-}17}$-7PO-sulfate, 0.5 wt% of $C_{20\text{-}24}$-AOS, and 4.0 wt% SBA for Oil A**

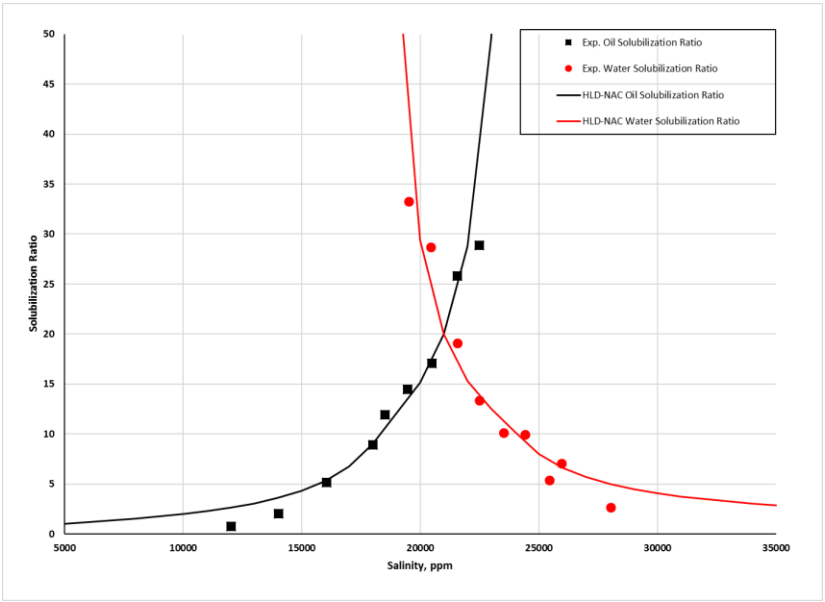


**Figure 11 HLD-NAC modeled phase behavior of a 0.5 wt% of $C_{13}$-13PO-sulfate, 0.5 wt% of $C_{20\text{-}24}$-IOS, and 2.0 wt% IBA for Oil B**

Figure 12 and Figure 13 showed experimental data from Chang et al. (2016). In Figure 12, the solubilization ratio of a 0.66 wt% of $C_{28}28(O) - 25PO - 25EO - COO$ and 0.3 wt% of $C_{15} - 18 - IOS$, 0.4 wt% of $C_{19} - 23 - IOS$ and 0.6 wt% $Phenol - 4EO$ for Oil C at 85 °$C$ was matched by the

HLD–NAC model coupled with the co-solvent partitioning model, and compared against the experimental data. Parameters were summarized as Formulation 4 in Table 3. The optimum salinity was 57,000 ppm, and the characteristic length was 395.1 Å. In Figure 13, the solubilization ratio of a 0.4 wt% of $C_{18} - 45PO - 30EO - COO$, 0.6 wt% of $C_{19} - 23 - IOS$ and 0.5 wt% of $Phenol - 2EO$ for Oil D at 85 $°C$ was matched and compared against the experimental data. Parameters were summarized as Formulation 5 in Tables 3. The optimum salinity was 30,000 ppm, and the characteristic length was 488.5 Å. For both formulations, experimental partition coefficients have been used, and the volumes of alcohol partitioning into the interfacial pseudo-phase for Formulation 4 and Formulation 5 were 0.045 wt% and 0.084 wt%, respectively.

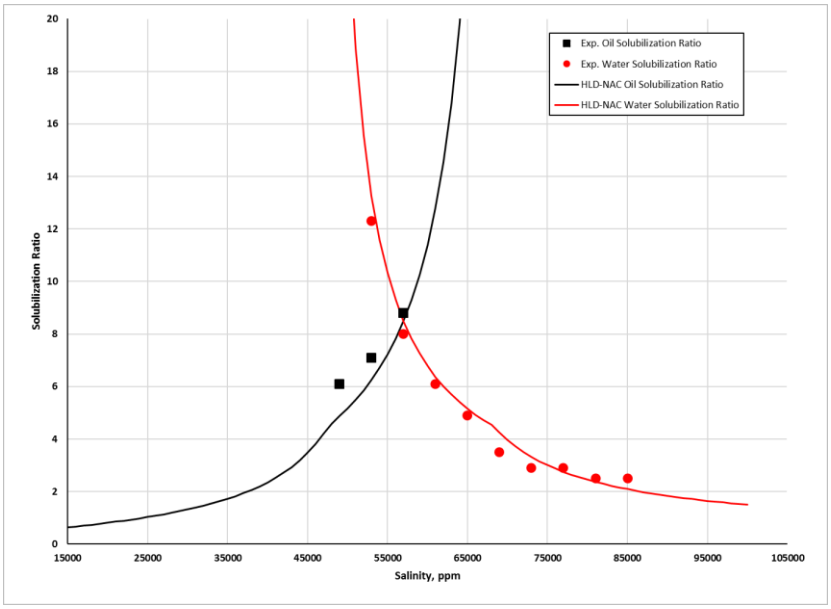


**Figure 12 HLD-NAC modeled phase behavior of a 0.66 wt% of $C_{28}$ (O)-25PO-25EO-COO, 0.3 wt% of $C_{15-18}$-IOS, 0.4 wt% of $C_{19-23}$-IOS and 0.6 wt% Phenol-4EO for Oil C**

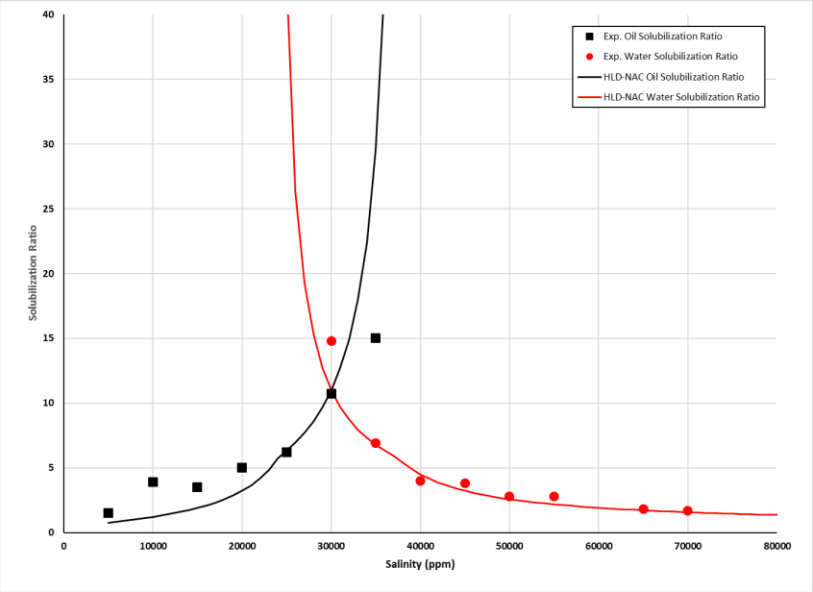


**Figure 13 HLD-NAC modeled phase behavior of a 0.4 wt% of $C_{18}$-45PO-30EO-COO, 0.6 wt% of $C_{19-23}$-IOS, and 0.5 wt% of Phenol-2EO for Oil D**

The results above have proven that the physics-based HLD-NAC equation of state coupled with the thermodynamic-based pseudophase model can successfully simulate the phase behavior of surfactant/co-solvent/oil/brine systems. The HLD-NAC model is capable of reproducing microemulsion phase behavior of various surfactant formulations with the only matching parameter, length parameter $L$. The length parameter is physically representing the surfactant tail length size. For the systems of formulations with co-solvents, more accurate length parameters can be obtained by considering that all co-solvents partition into brine, oil and surfactant phase instead of into surfactant phase only. The length parameter can be used to determine the model binodal curve in the ternary diagram. The more accurate length parameters are, the better binodal curves can be made in ternary diagrams to predict microemulsion compositions.

### 4.2 Model Binodal Curve with Catastrophic Phase Inversion Theory

Experimental data of binodal curves (Prouvost et al. 1984) for three different Winsor type systems were used to demonstrate the plotting procedures. The system consisted of brine, n-decane, 1.5% of Witco TRS 10-410 and 1.5% of IBA. Properties of Witco TRS 10-410 were given in Table 4. System formulation data were listed in Table 5. The length parameter was determined by the HLD-NAC model coupled with co-solvent partitioning model. Eq. 9b was employed to calculate the characteristic length $\xi^*$. Alcohol partition coefficient $K_A^O$ was calculated by Eq. 77, while $K_A^S$ was assumed based on the Acosta et al. (2003) and Acosta (2008).

The salinities used to make the ternary diagrams were 0.44, 1.2, and 1.85 wt% NaCl, which resulted in Type I, Type III and Type II phase behavior, respectively. The optimum salinity was 1.21 wt% NaCl. The experimental binodal curves were obtained from the phase volume readings, which were from the experiments that a set of 60 samples was made at each salinity. Accurate models of binodal curves were made by matching the experimental binodal curves so that microemulsion compisitions can be predicted after the specific systems reached equilibrium.

**Table 4 Properties of Witco TRS 10-410**

| Descriptive name | MW (g/mole) | Head area $a_s$, (Å$^2$) |
|---|---|---|
| Witco TRS 10-410 | 420 [a] | 60 [b] |

a: Obtained from reference (Hedges and Glinsmann 1979)

b: Obtained from reference (Rosen 2004)

**Table 5 Formulation summary for brine, n-decane, 1.5% of Witco TRS 10-410 and 1.5% of IBA system**

| System formulation | Oil | Optimum salinity $S^*$, wt% NaCl | Alcohol partition coefficients | | Characteristic length, $\xi^*$, Å | Length parameter, L, Å |
|---|---|---|---|---|---|---|
| | | | $K_A^O$ | $K_A^S$ | | |
| 1.5 wt % Witco TRS 10-410 and 1.5 wt% IBA | n-decane | 1.21 | 0.20 | 79 | 456.7 | 15 |

Figure 14 showed the Type I ternary diagram at the salinity of 0.44 wt% NaCl. The model binodal curve was made by two steps. Firstly, assuming the microemulsion at certain salinity has constant solubilization ratio as long as the overall composition lies in the multiphase region. The solubilization ratio was the slope of the longer part of the binodal curve connecting with the aqueous pseudo-phase apex. Therefore, the longer part of the binodal curver can be determined with the known slope and the starting point. Secondly, the catastrophic phase inversion theory was applied. The volume fraction of the internal phase inversion was assumed to be 75%, represented by the dash line in Figure 14. The dash line crossed the longer part of the binodal curve at the plait point. The binodal curve was completed when the plait point connected with the oleic pseudo-phase apex. The binodal curve separated the ternary diagram into two different regions. Below the curve was the two-phase region, while single-phase region was above the binodal curve. The physical meaning of the height of the plait point was the solubilization capability of the system. The higher the plait point was, the less solubilization capability the system had.

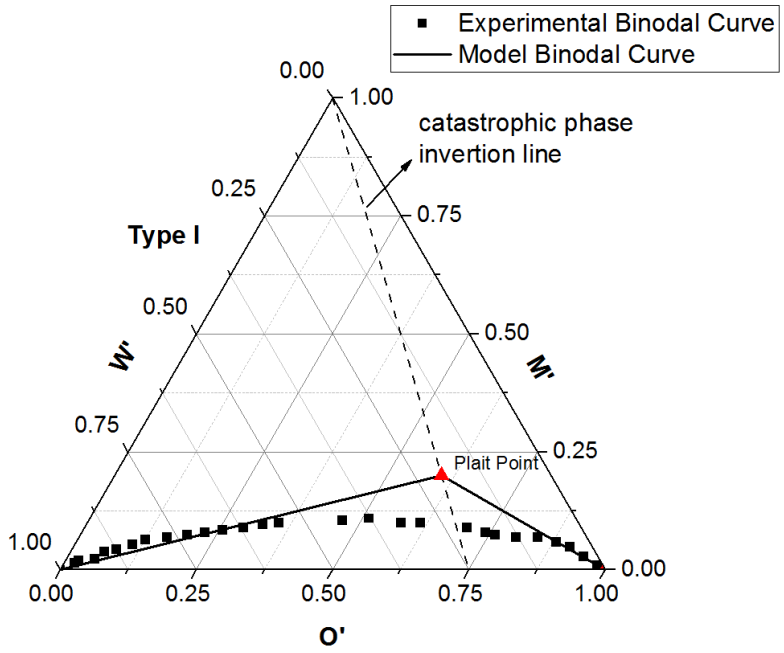


**Figure 14 Binodal curve with catastrophic theory for 1.5% of Witco TRS 10-410 and 1.5% of IBA for n-decane at 0.44 wt% NaCl system (Type I)**

Similar method was used to plot the binodal curve for the Type II system at the salinity of 1.85 wt% NaCl, shown in Figure 15. However, since the excessive phase in any Type II systems was aqueous pseudo-phase, the dash line representing catastrophic phase inversion line intercepted at 0.25 of the oleic pseudo-phase axis of the ternary diagram.

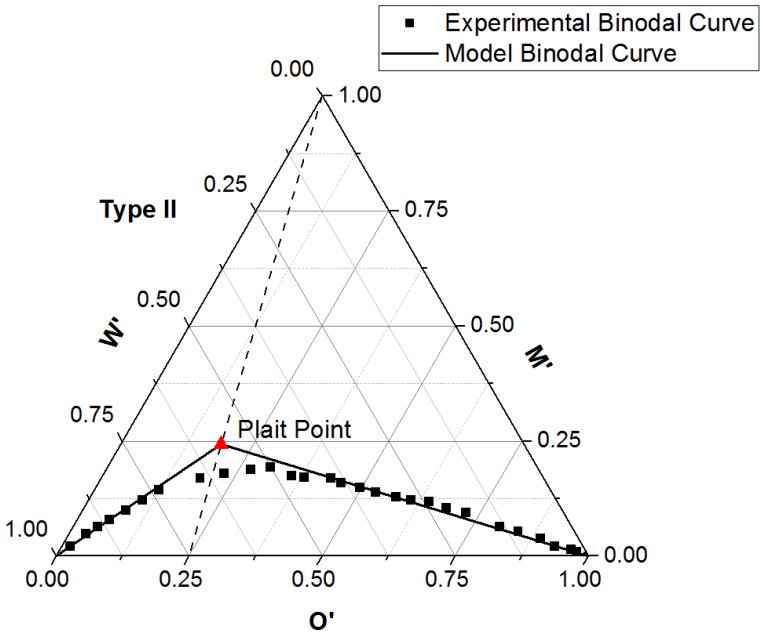


**Figure 15 Binodal curve with catastrophic theory for 1.5% of Witco TRS 10-410 and 1.5% of IBA for n-decane at 1.85 wt% NaCl system (Type II)**

In Figure 16, the ternary diagram was plotted at the salinity of 1.2 wt% NaCl. However, the optimum salinity for this system was 1.21 wt% NaCl. Therefore, the convergent point of the left lobe and right lobe from the experimental data was at the left side of the value of 0.5 for the oleic pseudo-phase axis. If the ternary diagram was plotted at the optimum salinity, the converge point should be the invariant point, which will split to a microemulsion with equal volume of brine and oil and two excess phases as the system was equilibrated. It is worth noting that both the microemulsion phase and two excess pahses did containt co-solvents. The overall composition placed in the Type I or Type II lobe as long as the volumes of initial brine and oil were less than the solubilization capability of the system. The microemulsion composition moved from the invariant point to one of the plait points along the binodal curve. The left lobe was

determined the same as the binodal curve of the Type II system, while the right lobe was determined the same as the binodal curve of the Type I system.

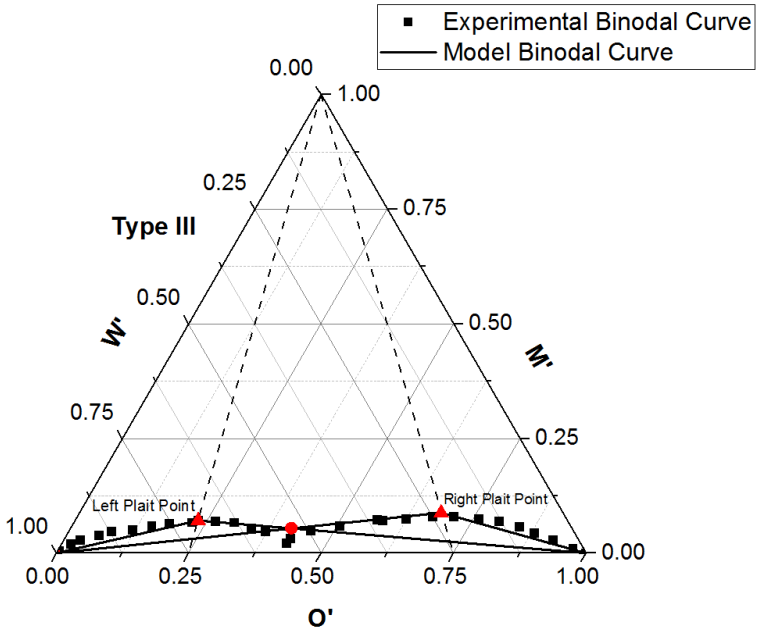


**Figure 16 Binodal curve with catastrophic theory for 1.5% of Witco TRS 10-410 and 1.5% of IBA for n-decane at 1.2 wt% NaCl system (Type III)**

### *4.2.1 Accuracy*

In Figure 14, when microemulsion was Type I, the model binodal curve was able to match the lower part of the experimental binodal curver. However, significant errors occurred as the height of the model binodal curve was much higher than the height of the experimental binodal curve. Thus, the model binodal curve underestimated the solubilization capability of the system. Similar result can be found when microemulsion was Type II, which was shown in Figure 15. Although, in the Type II system, the model binodal curve matched the experimental binodal curve better than that in the Type I system, the model binodal curve still underestimated the solubilization capability of the system. For

the Type III system, Figure 16 presented that the convergent point of the model left lobe and right lobe (the red dot) was significantly different from the convergent point of the experimental left lobe and right lobe, meaning that the model failed to predict the microemulsion compositions after the system reached equilibrium. The turning points for all model binodal curves were always the plait points. However, the turning points for the experimental binodal curves were located far away from the plait point in the ternary diagrams. Therefore, considering all the significant differences mentioned above, although catastrophic theory can be used to make binodal curves to predict microemulsion compositions to some extent, new methods should be developed to increase the accuracy of the model binodal curves.

### 4.3 Model Binodal Curve with The New Algorithm

Some experimental data were used in this section as those in the section of *4.2 Model Binodal Curve with Catastrophic Theory* to demonstrate the performance of the new algorithm which considers the effect of alcohol. The system consisted of brine, n-decane, 1.5% of Witco TRS 10-410 and 1.5% of IBA. Properties of Witco TRS 10-410 were given in Table 4. System formulation data were listed in Table 5. The salinities used to make the ternary diagrams were 0.44, 1.2, and 1.85 wt% NaCl, which resulted in Type I, Type III and Type II phase behavior, respectively. The optimum salinity was 1.21 wt% NaCl. The experimental binodal curves were obtained from the phase volume readings,

which were from the experiments that a set of 60 samples was made at each salinity.

The tuned values for $C_1$ and $C_2$ for the new algorithm were presented in Table 6.

**Table 6 Tuned values of $C_1$ and $C_2$ for brine, n-decane, 1.5% of Witco TRS 10-410 and 1.5% of IBA system**

| Coefficient | Type I | Type II | Type III | |
|---|---|---|---|---|
| | | | Left Lobe | Right Lobe |
| $C_1$ | 8 | 65 | 80 | 35 |
| $C_2$ | 0.015 | -0.012 | -0.032 | 0.08 |

### *4.3.1 Accuracy*

Figure 17 and Figure 18 indicated that the model binodal curves almost completely overlapped the experimental binodal curves, and that the new algorithm worked very well in making the continuous binodal curves for both Type I and Type II systems.

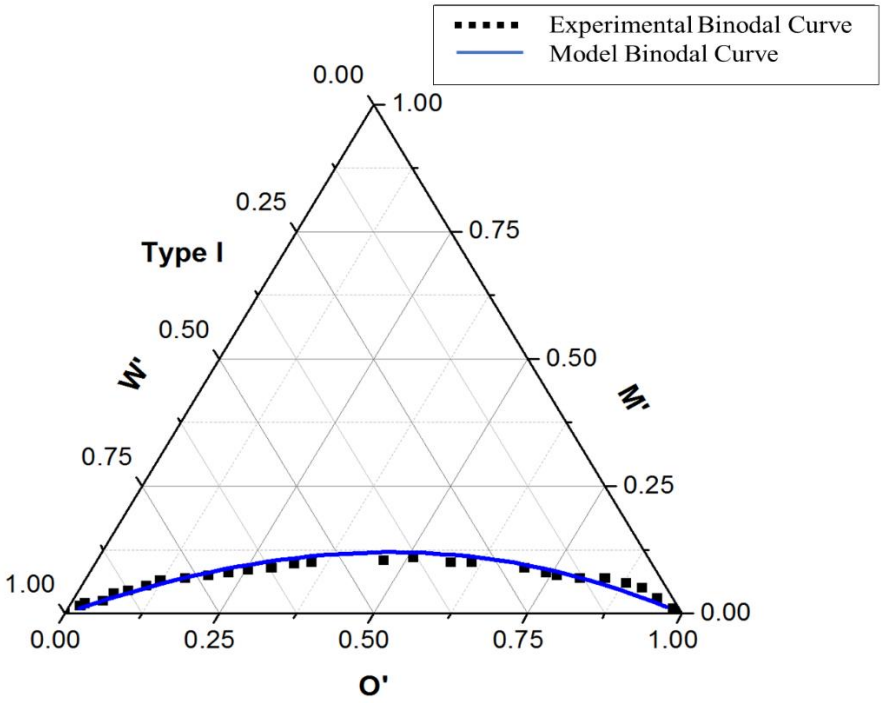


**Figure 17 Binodal curve with the new algorithm for 1.5% of Witco TRS 10-410 and 1.5% of IBA for n-decane at 0.44 wt% NaCl system (Type I)**

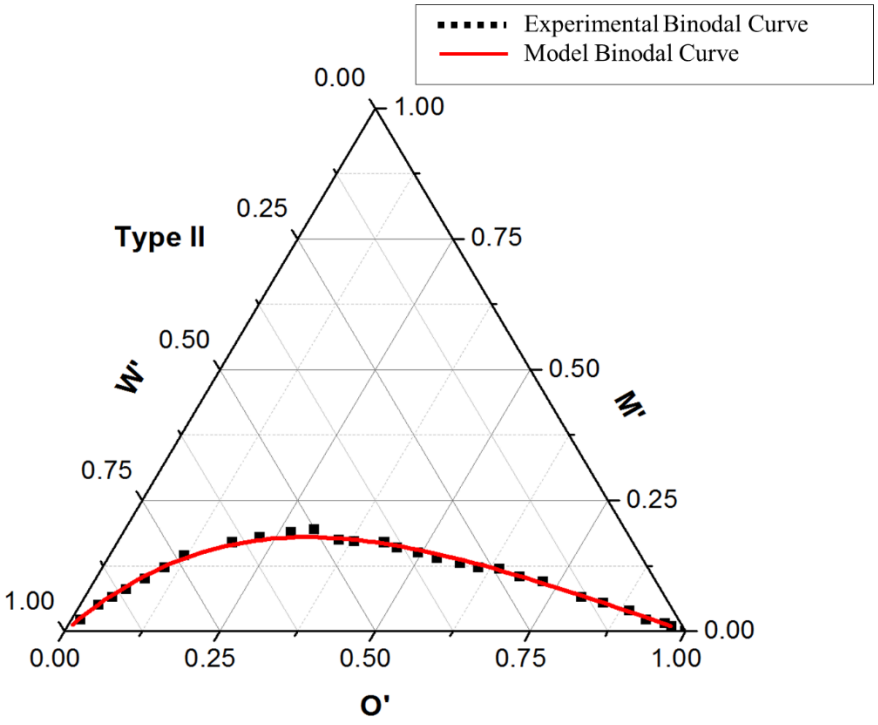


**Figure 18 Binodal curve with the new algorithm for 1.5% of Witco TRS 10-410 and 1.5% of IBA for n-decane at 1.85 wt% NaCl system (Type II)**

Although Figure 19 expressed that in the Type III system the algorithm tended to underestimate both left lobe and right lobe as they were converging, it successfully predicted the convergent point (the red dot), which was the volume fractions of each component in microemulsion phase after the system reached equilibrium. The red dot, representing the model's result, overlapped the convergent point of experimental left lobe and right lobe. Therefore, the three-phase region was successfully predicted for the Type III system.

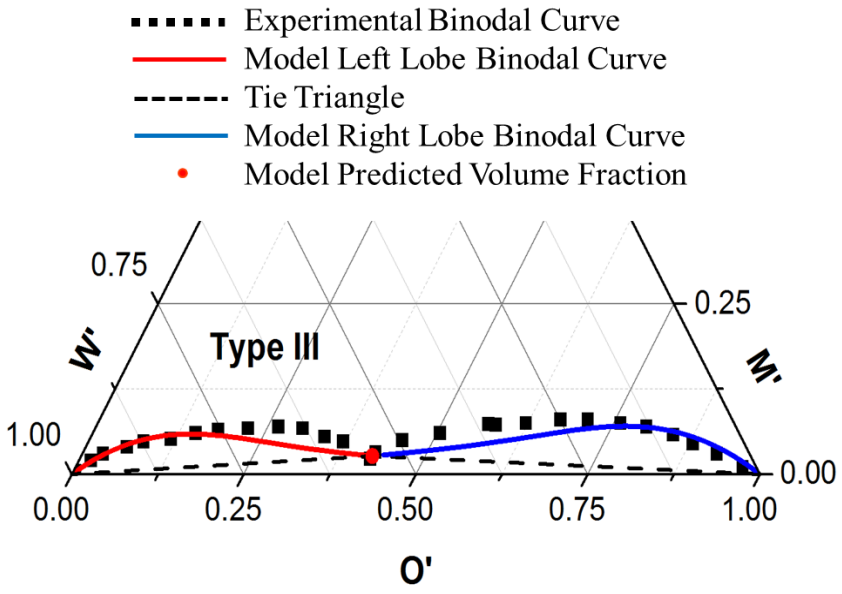


**Figure 19 Binodal curve with the new algorithm for 1.5% of Witco TRS 10-410 and 1.5% of IBA for n-decane at 1.2 wt% NaCl system (Type III)**

The results validated that the new algorithm, which considered the effects of co-solvent partitioning, can correctly model the microemulsion phase behavior for all Winsor types systems, and outperform the catastrophic phase inversion theory method.

# Chapter 5: Conclusions

The physics-based HLD-NAC equation of state coupled with the thermodynamic-based pseudo-phase model was employed to simulate the phase behavior of surfactant/co-solvent/oil/ brine systems. Algorithm of modeling the solubilization ratios and the method to predict phase volume fractions were demonstrated. Solubilization curves and ternary diagrams of single surfactant, surfactant mixtures with and without co-solvents for various types of crude oil were simulated, and conclusions were summarized:

1. The HLD-NAC model is capable of reproducing microemulsion phase behavior of various surfactant formulations with the only fitting parameter, length parameter L.
2. The length parameter is physically representing the surfactant tail length size. The value of length parameter increases as the surfactant or surfactant mixture has a longer tail length in the formulation. It can be determined by matching the experimental data of solubilization ratio.
3. The issue of underestimating the length parameters for formulations with co-solvents due to the erroneous consideration that all co-solvents were completely dissolved and adsorbed at the phase interface leading to an overestimated interfacial area has been addressed in this work. More accurate length parameters can be obtained by considering that all co-solvents partition into brine, oil and surfactant phases instead of into microemulsion phase only.

4. The length parameter can be used to determine the model binodal curves in the ternary diagram with catastrophic phase inversion theory. However, the model binodal curves created by catastrophic phase inversion theory are not able to reproduce the experimental binodal curves for the system with co-solvent correctly. Significant errors may occur when estimating the number of phases and the concentrations of compositions in microemulsion phase with the plotted ternary diagrams. Binodal curves with high accuracy are essential to the formulation designs for surfactant/co-solvent mixtures.
5. The Khorsandi and Johns' flash algorithm with consideration of phase partitioning of co-solvent can accurately simulate phase behavior of surfactant/co-solvent/crude oil/brine systems. The new algorithm is developed to advoid the use of catastrophic theory so that better model binodal curves can be generated in the ternary diagrams. A flow chart for the new algorithm as well as the results of tuning parameters are given and demonstrated.

Recommendations for future research

1. This study combined HLD-NAC with co-solvent partitioning model, which added one more component (co-solvent) into the HLD-NAC model. Further study may integrate this mode and chemical flooding simulators so that coreflood experiments for surfactant/co-solvent/oil/brine systems can be simulated.

2. Although Khorsandi and Johns' flash algorithm outperformed the catastrophic theory, it contains more empirical adjustment which undermines the physical significance of the HLD-NAC model. Thus, future study may focus on reducing these empirical features, however maintaining the accuracy of Khorsandi and Johns' flash algorithm.

3. In this study, Khorsandi and Johns' flash algorithm coupled the co-solvent partitioning was used to reproduce experimental data for the system with one single surfactant formulation. However, two or more surfactants (surfactant mixture) are usually used in formulation design. Future study many employ this method to match experimental data for systems containing surfactant mixture.

4. Future research could also examine values of partition coefficients for the formulations using the same surfactant or surfactant mixture but different co-solvents. Hence, the impacts of co-solvents partitioning with phases on microemulsion phase behavior may be better understood.

# References


Abrams, A., 1975. The influence of fluid viscosity, interfacial tension, and flow velocity on residual oil saturation left by waterflood. Society of Petroleum Engineers Journal, 15(05), 437-447.

Acosta, E. J., Kiran, S. K., Hammond, C. E., 2012. The HLD-NAC model for extended surfactant microemulsions. Journal of Surfactants and Detergents, 15(4), 495-504.

Acosta, E. J., Yuan, J. S., Bhakta, A. S., 2008. The characteristic curvature of ionic surfactants. Journal of Surfactants and Detergents, 11(2), 145-158.

Acosta, E., Szekeres, E., Sabatini, D. A., Harwell, J. H., 2003. Net-average curvature model for solubilization and supersolubilization in surfactant microemulsions. Langmuir, 19(1), 186-195.

Adkins, S., Gayani, P. A., Solairaj, S., Lu, J., Weerasooriya, U. P., Pope, G. A., 2012. Development of thermally and chemically stable lardge-hydrophobe alkoxy carboxylate surfactants. SPE Improved Oil Recovery Symposium. Society of Petroleum Engineers.

Bellocq, A. M., Bourbon, D., Lemenceau, B., 1981. Three-dimensional phase diagrams and interfacial tensions of the water-dodecane-pentanol-sodium octylbenzene sulfonate system. Journal of Colloid and Interface Science, 79(2), 419-431.

Biais, J., Bothorel, P., Clin, B., Lalanne, P., 1981. Theoretical behaviour of Microemulsions: Geometrical aspects, dilution properties and role of alcohol. Comparison with experimental result. Journal of Dispersion Science and Technology, 2(1), 67-95.

Blevins, C. E., Willhite, G. P., Michnick, M. J., 1981. Investigation of the three-phase regions formed by petroleum sulfonates. Society of Petroleum Engineers Journal, 21(05), 581-592.

Camilleri, D., 1983. Micellar/polymer flooding experiments and comparison with an improved 1-D simulator. Master's Thesis. The University of Texas at Austin.

Chang, L. Y., Lansakara-P, D. S. P., Jang, S. H., Weerasooriya, U. P., Pope, G. A., 2016. Co-solvent Partitioning and Retention. SPE Improved Oil Recovery Conference. Society of Petroleum Engineers.

Chou, S. I., Bae, J. H., 1988. Phase-behavior correlation for high-salinity surfactant formulations. SPE reservoir engineering, 3(03), 778-790.

De Gennes, P. G., Taupin, C., 1982. Microemulsions and the flexibility of oil/water interfaces. The Journal of Physical Chemistry, 86(13), 2294-2304.

Delshad, M., Pope, G. A., Sepehrnoori, K., 1996. A compositional simulator for modeling surfactant enhanced aquifer remediation, 1 formulation. Journal of Contaminant Hydrology, 23(4), 303-327.

Dominguez, J. G., Willhite, G. P., Green, D. W., 1979. Phase behavior of microemulsion systems with emphasis on effects of paraffinic hydrocarbons and alcohols. Solution Chemistry of Surfactants, 2, 673-697.

Dwarakanath, V., Pope, G. A., 1998. New approach for estimating alcohol partition coefficients between nonaqueous phase liquids and water. Environmental Science & Technology, 32(11), 1662-1666.

Ghosh, S., Johns, R. T., 2016. A dimensionless equation of state to predict microemulsion phase behavior. Langmuir, 32(35), 8969-8979.

Ghosh, S., Johns, R. T., 2014. A New HLD-NAC Based EOS Approach to Predict Surfactant-Oil-Brine Phase Behavior for Live Oil at Reservoir Pressure and Temperature. SPE Annual Technical Conference and Exhibition. Society of Petroleum Engineers.

Glinsmann, R. G., 1979. Surfactant flooding with microemulsions formed in-situ-effect of oil characteristics. SPE Annual Technical Conference and Exhibition. Las Vegas, Nevada.

Goudarzi, A., Delshad, M., Sepehrnoori, K., 2016. A chemical EOR benchmark study of different reservoir simulators. Computers & Geosciences, 94, 96-109.

Green, D.W., Willhite. G. P., 1998. Enhanced Oil Recovery. Henry L. Doherty Memorial Fund of AIME. Society of Petroleum Engineer.

Griffin, W. C., 1949. Classification of surface-active agents by HLB. Journal of the Society of Cosmetic Chemists, 1, 311-326.

Hammond, C. E., Acosta, E. J., 2012. On the characteristic curvature of alkylpolypropylene oxide sulfate extended surfactants. Journal of Surfactants and Detergents, 15(2), 157-165.

Hand, D. B., 1939. The distribution of a consulate liquid between two immiscible liquids. The Journal of Physical Chemistry, 34, 1961-2000.

Hedges, J. H., Glinsmann, G. R., 1979. Compositional effects on surfactantflood optimization. SPE Annual Technical Conference and Exhibition. Las Vegas, Nevada.

Hirasaki, G. J., 1982. Interpretation of the change in optimal salinity with overall surfactant concentration. Society of Petroleum Engineers Journal, 22(06), 971-982.

Jin, L., Budhathoki, M., Jamili, A., Li, Z., Luo, H., Shiau, B. J. Ben, Delshad, M., Harwell, J. H., 2016a. Predicting microemulsion phase behavior using physics based HLD-NAC equation of state for surfactant flooding. Journal of Petroleum Science and Engineering.

Jin, L., Li, Z., Jamili, A., Lu, J., Delshad, M., Shiau, B. J. Ben, Harwell, J. H., Rui, Z., 2016b. Development of a chemical flood simulator based on predictive HLD-NAC equation of state for surfactant. SPE Annual Technical Conference and Exhibition. Dubai, UAE.

Jin, L., Jamili, A., Li, Z., Lu, J., Luo, H., Shiau, B. J. Ben, Harwell, J. H., 2015. Physics based HLD-NAC phase behavior model for surfactant/crude oil/brine systems." Journal of Petroleum Science and Engineering, 136, 68-77.

Khorsandi, S., Johns, T. R., 2016. Robust flash calculation algorithm for microemulsion phase behavior. Journal of Surfactants and Detergents, 19, 1273-1287.

Levitt, D. B., Jackson, A. C., Heinson, C., Britton, L. N., Malik, T., Dwarakanath, V., Pope, G. A., 2009. Identification and Evaluation of High Performance EOR Surfactants. SPE Reservoir Evaluation & Engineering, 12(02), 243-253.

Lu, J., Britton, C., Solairaj, S., Liyanage, P. J., Kim, D. H., Adkins, S., Pope, G. A., 2014a. Novel large-hydrophobe alkoxy carboxylate surfactants for enhanced oil recovery. Society of Petroleum Engineers Journal, 19(06), 1024-1034.

Lu, J., Weerasooriya U. P., Pope, G. A., 2014b. Investigation of gravity-stable surfactant floods. Fuel, 124(15), 76-84.

Lu, J., Liyanage P. J., Solairaj, S., Adkins, S., Gayani P. A., Kim, D. H., Britton, C., Weerasooriya, U. P., Pope, G. A., 2014c. New surfactant developments for chemical enhanced oil recovery. Journal of Petroleum Science and Engineering, 120, 94-101.

Melrose, J. C., 1974. Role of capillary forces in detennining microscopic displacement efficiency for oil recovery by waterflooding. Journal of Canadian Petroleum Technology, 13(04).

Mitchell, D. J., Ninham, B. W., 1981. Micelles, vesicles and microemulsions. Journal of the Chemical Society, Faraday Transactions 2: Molecular and Chemical Physics, 77(4), 601-629.

Nelson, R. C., Pope, G. A., 1978. Phase relationships in chemical flooding. Society of Petroleum Engineers Journal, 18(5), 325-338.

Prouvost, L. P., Satoh, T., Sepehrnoori, K., Pope, G. A., 1984. A new micellar phase-behavior model for simulating system with up to three amphiphilic species. SPE Annual Technical Conference and Exhibition. Houston, Texas.

Prouvost, L., Pope, G. A., Rouse, B., 1985. Microemulsion phase behavior: a thermodynamic modeling of the phase partitioning of amphiphilic species. Society of Petroleum Engineers Journal, 25(05), 693-703.

Puerto, C. M., Reed, L. R., 1983. A three-parameter representation of surfactant/oil/brine interaction. Society of Petroleum Engineers Journal, 23(04), 669-682.

Rosen, M. J., 2004. Surfactants and interfacial phenomena. 3rd ed. New York, John Wiley & Sons.

Salager, J. L., Anton R. E., 1999. Hankbook of Microemulsion Science and Technology. 247-280. New York, Kumar, P., Mittal, K. L., Eds.; Marcel Dekker.

Salager, J. L., Marquez, N., Graciaa, A., Lachaise, J., 2000a. Partitioning of ethoxylated octylphenol surfactants in microemulsion-oil-water systems: influence of temperature and relation between partitioning coefficient and physicochemical formulation. Langmuir, 16(13), 5534-5539.

Salager, J. L., Marquez, L., Pena, A. A., Rondon, M., Silva, F., Tyrode, E., 2000b. Current phenomenological know-how and modeling of emulsion inversion. Industrial & Engineering Chemistry Research, 39(8), 2665-2676.

Salager, J. L., Miñana-Pérez, M., Pérez-Sánchez, M., Ramfrez-Gouveia, M., Ramfrez-Gouveia, M., Rojas, C. I., 1983. Surfanctant-oil-water systems near the affinity inversion Part III: The two kinds of emulsion inversion. Journal of Dispersion Science and Technology, 4(3), 313-329.

Salager, J. L., Morgan, J. C., Schechter, R. S., Wade, W. H., Vasquez, E., 1979. Optimum formulation of surfactant/water/oil systems for minimum interfacial tension or phase behavior. Society of Petroleum Engineers Journal, 19(2), 107-115.

Salager, S. E., Tyrode, E. C., Celis, M. T., Salager, J. L., 2001. Influence of the stirrer initial position on emulsion morphology. Making use of the local water-to-oil ratio concept for formulation engineering purpose. Industrial & Engineering Chemistry Research, 40(22), 4808-4814.

Salter, S. J., 1978. Selection of pseudo-components in surfactant-oil-brine-alcohol systems. The Fifth Symposium on Improved Methods for Oil Recovery of the Society of Petroleum Engineers of AIME. Tulsa, Oklahoma.

Sheng, J., 2010. Modern Chemical Enhanced Oil Recovery: Theory and Practice. Elsevier Science.

Stegemeier, G. L., 1977. Mechanisms of entrapment and mobilization of oil in porous media. In Improved Oil Recovery by Surfactant and Polymer Flooding, 55-91.

Taber, J. J., 1969. Dynamic and static forces required to remove a discontinuous oil phase from porous media containing both oil and water. Society of Petroleum Engineers Journal, 9(01), 3-12.

Trahan, G., Nguyen, T., and Jakobs-Sauter, B., 2015. Applying the Hydrophilic-Lipophilic Deviation (HLD) Concept to Chemical EOR Formulations. 18th European Symposium on Improved Oil Recovery. Dresden, Germany.

Troncoso, A. B., Acosta, E., 2015. Van der Waals free energy model for solubilization of oil in micelles. Soft Matter, 11(3), 516-531.

Vinatieri, J. E., Fleming III, P. D., 1979. The use of pseudocomponents in the representation of phase behavior of surfactant systems. Society of Petroleum Engineers Journal, 19(05), 289-300.

Wickert B. L., Willhite, G. P., Green, D. W. Black, S. L., 1978. Interfacial and phase behavior of a microemulsion system using a quaternary diagram. A.I.Ch.E. 85th National Meeting. Philadelphia, Pennylvania.

Winsor, P. A., 1948. Hydrotropy, solubilization and related emulsification processes. Transactions of the Faraday Society, 44, 376-398.

# Appendix A: Nomenclature

*Roman*

| | | |
|---|---|---|
| $A$ | : | Characteristic Length Interpolation Coefficient |
| $A, B, C, D$ | : | Coefficients for One-alcohol Cubic Equation |
| $a$ | : | Ratio of Molar Volume of Monomeric Alcohol A to Equivalent Molar Volume of Surfactant |
| $a_-$ | : | Type I Tie Line Slope |
| $a_+$ | : | Type II Tie Line Slope |
| $a_{s_i}$ | : | Surface Area per Molecule of the Surfactant $i$ ($Å^2$) |
| $A_s$ | : | Total Interfacial Area in Microemulsion ($Å^2$) |
| $a_-^c$ | : | Type I Limiting Tie Line Slope |
| $a_+^c$ | : | Type II Limiting Tie Line Slope |
| $a_-^*$ | : | Slope for Left Boundary of Tie Triangle |
| $a_+^*$ | : | Slope for Right Boundary of Tie Triangle |
| $b$ | : | Ratio of Molar Volume of Monomeric Alcohol B to Equivalent Molar Volume of Surfactant |
| $b_-$ | : | Type I Tie Line Interception |
| $b_+$ | : | Type II Tie Line Interception |
| $b_-^c$ | : | Type I Limiting Tie Line Interception |
| $b_+^c$ | : | Type II Limiting Tie Line Interception |
| $b_-^*$ | : | Interception for Left Boundary of Tie Triangle |
| $b_+^*$ | : | Interception for Right Boundary of Tie Triangle |
| $C_1$ | : | Coefficient for Critical Characteristic Length |

| | | |
|---|---|---|
| $C_2$ | : | Coefficient for Critical Characteristic Length |
| $Cc$ | : | Characteristic Curvature |
| $C_O^M$ | : | Volume Fraction of Oil in the Middle Phase Microemulsion |
| $C_S^M$ | : | Volume Fraction of Surfactant in the Middle Phase Microemulsion |
| $C_W^M$ | : | Volume Fraction of Brine in the Middle Phase Microemulsion |
| CMC | : | Critical Micelle Concentration |
| $C_{s_i}$ | : | Concentration of Each Surfactant or Co-solvent $i$ |
| $EACN$ | : | Equivalent Alkane Carbon Number (EACN unit) |
| $EACN_{alcohol}$ | : | Alcohol Equivalent Alkane Carbon Number (EACN unit) |
| $EACN_{oil}$ | : | Crude Oil Equivalent Alkane Carbon Number (EACN unit) |
| EOR | : | Enhanced Oil Recovery |
| EOS | : | Equation of State |
| $f(A)$ | : | Function of Alcohol Type and Concentration |
| $H_a$ | : | Average Curvature ($Å^{-1}$) |
| HLD | : | Hydrophilic Lipophilic Difference |
| $H_n$ | : | Nut Curvature ($Å^{-1}$) |
| $H'$ | : | $2/\xi_D^*$ |
| $I$ | : | $I - ratio$ |
| IBA | : | Isobutyl Alcohol |
| IFT | : | Interfacial Tension |
| $K$ | : | Slope of the Logarithm of Optimum Salinity as a Function of EACN (per EACN unit) |

| | | |
|---|---|---|
| $k_w$ | : | Partition Coefficient of Monomeric Alcohol between Aqueous and Oleic Pseudo-phases |
| $k_m$ | : | Partition Coefficient of Monomeric Alcohol between Interfacial and Oleic Pseudo-phases |
| $K_1$ | : | Self-association Constant of Monomeric Alcohol A in Oleic Pseudo-phase |
| $K_A^O$ | : | Partition Coefficient, $\gamma/\lambda$ |
| $K_S^O$ | : | Partition Coefficient, $\sigma/\lambda$ |
| $L$ | : | Surfactant Length Parameter (Å) |
| $MW_i$ | : | Molecular Weight ($g/mol$) |
| $N_a$ | : | Avogadro Number, $6.023\times10^{23}\ mol^{-1}$ |
| NAC | : | Net-Average Curvature |
| $P$ | : | Pressure (bar) |
| $R_O$ | : | Radius of Hypothetical Oil Droplet in Microemulsion (Å) |
| $R_W$ | : | Radius of Hypothetical Water Droplet in Microemulsion (Å) |
| S | : | Salinity ($g/100mL$) |
| $S^*$ | : | Optimum Salinity ($g/100mL$) |
| SBA | : | Secondary Butyl Alcohol |
| T | : | Temperature ($K$) |
| $V_A$ | : | Overall Alcohol A Volume in a System ($mL$) |
| $V_B$ | : | Overall Alcohol B Volume in a System ($mL$) |
| $V_m$ | : | Volume of the Middle Phase |
| $V_O$ | : | Overall Oil Volume in a System ($mL$) |

$V_{po}$ : Volume of Oil and Alcohol Associated with Oil

$V_{ps}$ : Volume of Surfactant and Alcohol Associated with Surfactant

$V_{pw}$ : Volume of Brine and Alcohol Associated with Brine

$V_S$ : Overall Surfactant Volume in a System ($mL$)

$V_W$ : Overall Water Volume in a System ($mL$)

$V_A^{M\prime}$ : Volume of Association of Alcohol to Interfacial Pseudo-phase

$V_A^{O\prime}$ : Volume of Association of Alcohol to Oleic Pseudo-phase

$V_A^{W\prime}$ : Volume of Association of Alcohol to Aqueous Pseudo-phase

*Greek*

$\alpha_T$ : Temperature Coefficient of Optimum Salinity ($K^{-1}$)

$\beta$ : Pressure Coefficient ($bar^{-1}$)

$\gamma$ : Ratio of $V_A^{O\prime}$ and $V_O$, $V_A^{O\prime}/V_O$

$\lambda$ : Ratio of $V_A^{W\prime}$ and $V_W$, $V_A^{W\prime}/V_W$

$\xi$ : Characteristic Length (Å)

$\xi_D$ : Dimensionless Characteristic Length

$\xi_D^{\mathrm{c}}$ : Dimensionless Characteristic Length for Limiting Tie Line

$\xi^*$ : Characteristic Length for Optimum Formulation (Å)

$\xi_D^*$ : Dimensionless Characteristic Length for Optimum Formulation

$\rho_i$ : Density of the Surfactant or Co-solvent $i$ ($g/mL$)

$\sigma$ : Ratio of $V_A^{M\prime}$ and $V_S$, $V_A^{M\prime}/V_S$

$\sigma_o$ : Solubilization Ratio of Oil

$\sigma_w$ : Solubilization Ratio of Brine Water

$\sigma_o^c$ : Solubilization Ratio of Oil at Limiting Condition

$\sigma_w^c$ : Solubilization Ratio of Brine Water at Limiting Condition

$\sigma_o^i$ : Solubilization Ratio of Oil at Initial Condition

$\sigma_w^i$ : Solubilization Ratio of Brine Water at Initial Condition

$\sigma_O^*$ : Optimum Solubilization Ratio of Oil

$\sigma_W^*$ : Optimum Solubilization Ratio of Brine Water